

Water Resources Research

RESEARCH ARTICLE

10.1029/2020WR027178

Key Points:

- A clay-capped Pleistocene aquifer under the influence of municipal pumping is contaminated with arsenic (As)
- After pumping started, breaks in the clay aquitard became conduits for accelerated transport of tritium, As, and carbon from the shallow aquifer
- Pumping induced transport of reactive carbon or arsenic emanating from the clay aquitard itself could lead to local release of As

Supporting Information:

- Supporting Information S1

Correspondence to:

M. R. H. Mozumder,
mozumder@ldeo.columbia.edu;
rmozumder@gradientcorp.com

Citation:








Mozumder, M. R. H., Michael, H. A., Mihajlov, I., Khan, M. R., Knappett, P. S. K., Bostick, B. C., et al. (2020). Origin of groundwater arsenic in a rural Pleistocene aquifer in Bangladesh depressurized by distal municipal pumping. *Water Resources Research*, 55, e2020WR027178. <https://doi.org/10.1029/2020WR027178>

Received 19 JAN 2020

Accepted 30 APR 2020

Accepted article online 6 MAY 2020

Origin of Groundwater Arsenic in a Rural Pleistocene Aquifer in Bangladesh Depressurized by Distal Municipal Pumping

M. R. H. Mozumder^{1,2} , H. A. Michael³ , I. Mihajlov^{1,4} , M. R. Khan⁵, P. S. K. Knappett⁶ , B. C. Bostick¹ , B. J. Mailloux⁷ , K. M. Ahmed⁵, I. Choudhury⁵, T. Koffman^{1,8} , T. Ellis¹, K. Whaley-Martin^{9,10}, R. San Pedro⁹, G. Slater⁹, M. Stute^{1,7}, P. Schlosser^{1,11}, and A. van Geen¹

¹Lamont-Doherty Earth Observatory of Columbia University, Palisades, NY, USA, ²Now at Gradient, Boston, MA, USA, ³Department of Earth Sciences, University of Delaware, Newark, DE, USA, ⁴Now at Geosyntec Consultants, Huntington Beach, CA, USA, ⁵Department of Geology, University of Dhaka, Dhaka, Bangladesh, ⁶Geology & Geophysics, Texas A&M University, College Station, TX, USA, ⁷Environmental Science, Barnard College, New York, NY, USA, ⁸Now at Land Resources and Environmental Sciences, Montana State University, Bozeman, MT, USA, ⁹Earth and Environmental Sciences, McMaster University, Hamilton, Ontario, Canada, ¹⁰Now at Civil and Mineral Engineering Department, University of Toronto, Ontario, Canada, ¹¹Now at Julie Ann Wrigley Global Institute of Sustainability, Arizona State University, Tempe, AZ, USA

Abstract Across South Asia, millions of villagers have reduced their exposure to high-arsenic (As) groundwater by switching to low-As wells. Isotopic tracers and flow modeling are used in this study to understand the groundwater flow system of a semi-confined aquifer of Pleistocene (>10 kyr) age in Bangladesh that is generally low in As but has been perturbed by massive pumping at a distance of about 25 km for the municipal water supply of Dhaka. A 10- to 15-m-thick clay aquitard caps much of the intermediate aquifer (>40- to 90-m depth) in the 3-km² study area, with some interruptions by younger channel sand deposits indicative of river scouring. Hydraulic heads in the intermediate aquifer below the clay-capped areas are 1–2 m lower than in the high-As shallow aquifer above the clay layer. In contrast, similar heads in the shallow and intermediate aquifer are observed where the clay layer is missing. The head distribution suggests a pattern of downward flow through interruptions in the aquitard and lateral advection from the sandy areas to the confined portion of the aquifer. The interpreted flow system is consistent with ³H-³He ages, stable isotope data, and groundwater flow modeling. Lateral flow could explain an association of elevated As with high methane concentrations within layers of gray sand below certain clay-capped portions of the Pleistocene aquifer. An influx of dissolved organic carbon from the clay layer itself leading to a reduction of initially orange sands has also likely contributed to the rise of As.

1. Introduction

Groundwater contamination with arsenic (As) threatens the health of more than 200 million people around the world who are exposed to As in drinking water that exceeds the World Health Organization (WHO) guideline of 10 μg/L (WHO, 1993; Ravenscroft et al., 2009). Bangladesh, part of the largest river delta in the world (Morgan & McIntire, 1959), is most affected with a rural population of about 40 million who are still exposed to As levels that exceed the WHO guideline by a factor of up to a hundred (BBS/UNICEF, 2011; BGS/DPHE, 2001; Smith et al., 2000). Spatial heterogeneity complicates the prediction of the distribution of As in the shallow (<50 m deep) Holocene (<12 kyr) aquifers of Bangladesh (Fendorf et al., 2010; van Geen et al., 2003), but older, deeper (>100 m) Pleistocene aquifers are consistently low in As in many parts of the region (BGS/DPHE, 2001; Burgess et al., 2010; Choudhury et al., 2016; Khan et al., 2019; Lapworth et al., 2018; Mihajlov et al., 2016; Ravenscroft et al., 2013). Aquifers in the Holocene-Pleistocene transition (50- to 100-m depth) are often also low in As and are increasingly exploited by local drillers contracted privately by individual households (Hossain et al., 2014; van Geen et al., 2006; von Brömssen et al., 2007). However, these intermediate aquifers could be more vulnerable to contamination than deep groundwater due to their proximity to shallow As contaminated aquifers (McArthur et al., 2008, 2011, 2016; Michael & Khan, 2016). Studying the geochemical and hydrologic processes that regulate groundwater As within this intermediate zone over time is therefore particularly relevant to

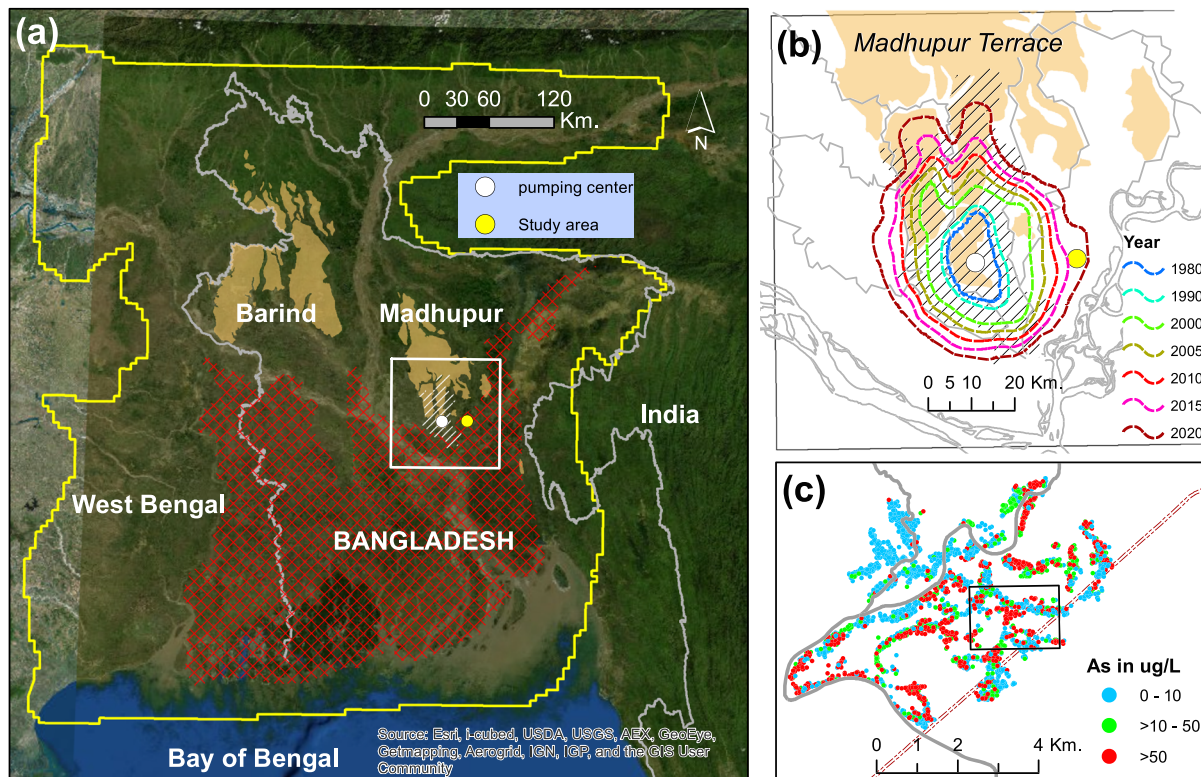


Figure 1. Study area. (a) Location of the study area with respect to Dhaka pumping center; the white rectangle shows the boundary of the child model of Khan et al. (2016); the perimeter of the basin-scale parent model of Michael and Voss (2008) is drawn in yellow; red cross-hatching indicates areas elevated in arsenic (As); orange polygons are the known regions of low-As Pleistocene aquifers exposed near the surface. (b) Simulated expansion of the 9-m water level depth (maximum suction limit for hand pumped wells) at a depth of 150 m over time (Khan et al., 2016). (c) The heterogeneous distribution of As in Araihaazar based on field-testing campaign carried out in 2017–2018. The rectangle shows our focus area of investigation (see Figure 2).

private well installations to reduce exposure (Jamil et al., 2019). In contrast to these private initiatives, government policy so far has relied primarily on nationwide installation of deep tubewells (Ravenscroft et al., 2009, 2013, 2014, 2018) that are too costly for most households.

Elevated levels of As ($>100 \mu\text{g/L}$) in shallow groundwater across the Ganges-Brahmaputra Delta have been widely attributed to microbially mediated reductive dissolution of iron(oxy)hydroxides (Ahmed et al., 1998, 2004; Berg et al., 2001; Bhattacharya et al., 1997; BGS/DPHE, 2001; Islam et al., 2004; McArthur et al., 2001; Nickson et al., 1998; Oremland & Stolz, 2003, 2005; Swartz et al., 2004; van Geen et al., 2004). There is, however, still no consensus about the source of labile carbon that is necessary for such reduction to take place (Harvey et al., 2002; Mailloux et al., 2013; Mladenov et al., 2010; Neumann et al., 2010; Polizzotto et al., 2008; Postma et al., 2012; Rowland et al., 2007; Whaley-Martin et al., 2016). Buried peat/coal fragments elevated in total organic carbon that were deposited extensively in the Bengal Basin during the last marine transgression could be an important source (McArthur et al., 2001, 2004; Rotiroti et al., 2014). A shallow marine environment during the Holocene transgression also favored the deposition of a thick sequence of clay that typically separates shallow high-As groundwater from the confined low-As aquifers. However, the clay aquitard itself may contain 1–3 orders of magnitude higher levels of dissolved organic carbon (DOC) than the sandy aquifers (Hendry & Wassenaar, 2000, 2005) which may diffuse and/or advect into the underlying aquifer and affect groundwater at the aquifer-aquitard interface (Hendry & Schwartz, 1990; Hendry et al., 2003; McMahon, 2001; McMahon & Chapelle, 1991).

In perturbed aquifers, the groundwater flow system is also likely to play an important role in redistributing As and reactive carbon (Burgess et al., 2010; Desbarats et al., 2014, 2017; Fendorf et al., 2010; MacDonald et al., 2016; Michael & Voss, 2008; Mihajlov et al., 2016; Mukherjee et al., 2011; Postma et al., 2017; van Geen et al., 2013; Winkel et al., 2011). Advection of As and young reactive carbon with surface recharge and groundwater flow has been invoked as the cause of contamination of some low-As aquifers (Klump

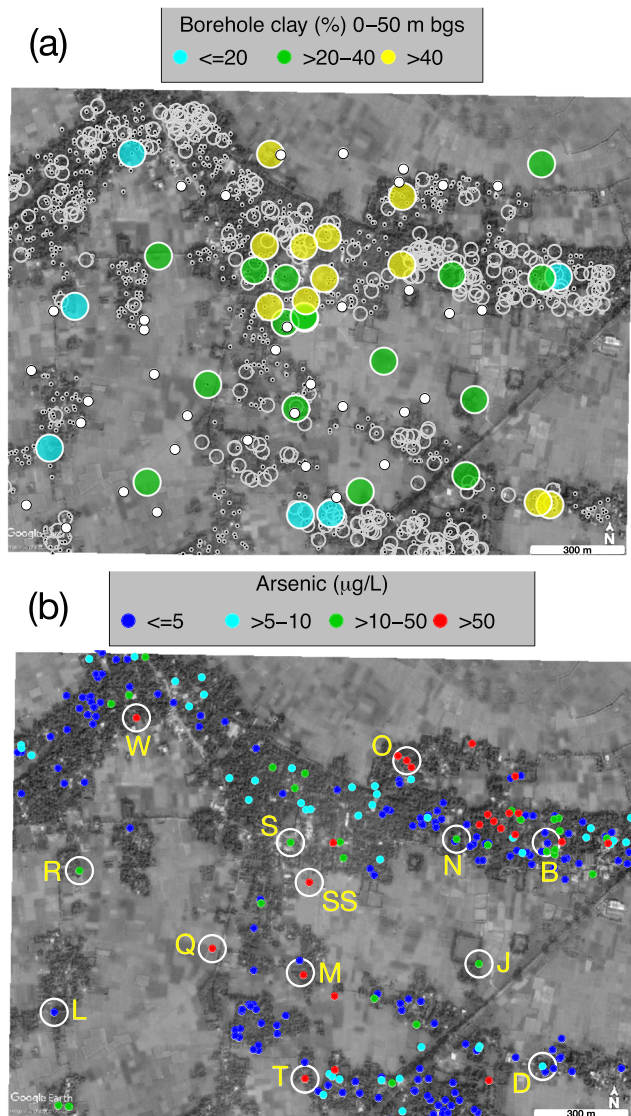


Figure 2. Geological and chemical heterogeneity in the study area. (a) The proportion of clay facies to a depth of 50 m below ground surface (bgs) at monitoring well locations. Also shown is the distribution of all hand pumps and irrigation wells. Small dots represent the shallow and deep wells, and gray open circles represent intermediate depth wells. The white filled circles indicate the locations of irrigation wells in the area. (b) Spatial distribution of arsenic in the intermediate aquifer (40–100 m bgs). Locations of the lettered monitoring sites are indicated with white open circles. A Google Earth image was used in the background.

et al., 2006; Lawson et al., 2013; Mailloux et al., 2013; Neumann et al., 2010; Polizzotto et al., 2005, 2008; Stahl et al., 2016; Whaley-Martin et al., 2016). The shallow aquifer of Bangladesh is perturbed by widespread irrigation pumping for growing rice (Harvey et al., 2002, 2006; Shamsudduha et al., 2011, 2015). In confined deeper aquifers within a 30- to 40-km radius of Dhaka, however, water levels have been falling rapidly under the influence of deep pumping for the city's municipal water supply since the 1980s (Ahmed et al., 1999; Hoque et al., 2007; IWM and DWASA, 2011; Khan et al., 2016; Knappett et al., 2016). The Dhaka cone of depression has expanded beyond the city limits, resulting in hydraulic gradients that could draw As and/or dissolved organic carbon into aquifers previously low in As (Khan et al., 2016; Knappett et al., 2016). Groundwater depletion has also been experienced by many other regions in the United States (e.g., High Plains and Central Valley of California aquifers), South and Central Asia (e.g., Indus Basin in Pakistan, northwestern India), North China Plain (e.g., the Hai River Basin), North Africa (e.g., North-Western Sahara Aquifer System), Middle East (e.g., Sa'dah Plain, Yemen), Europe (Altiplano region in Murcia, Spain), Australia (e.g., Great Artesian Basin, Gngangara Groundwater System), and other localized areas around the world (Famiglietti, 2014; Konikow and Kendy, 2005; Wada et al., 2010; Werner et al., 2013).

Large-scale (tens to hundreds of kilometers) numerical models have previously been used to assess the risk of anthropogenic contamination of deep (>150 m) low-As groundwater to downward advection of high-As groundwater (Hoque & Burgess, 2012; Hoque et al., 2017; Jusseret et al., 2009; Khan et al., 2016, 2019; Michael & Khan, 2016; Michael and Voss 2008; Radloff et al., 2011; Sahu et al., 2013; Shamsudduha et al., 2019; von Brömssen et al., 2014). However, such models have not been widely applied at finer resolution to understand the impacts of regional processes, like the growth of the Dhaka drawdown cone on local flow patterns and their impacts on long-term hydrogeochemical processes.

In the present study, we document the distal impact of Dhaka pumping on the evolution of the local hydrology and distribution of dissolved As within a vulnerable intermediate aquifer (>40–100 m) in a 3-km² area of Araihaazar, Bangladesh. We rely on long-term geochemical observations and develop a groundwater flow model constrained by head measurements and verified against isotopic tracers to shed light on the processes that evidently already led to the contamination of some portions of the intermediate aquifer, and to make future predictions.

2. Geologic Setting

The study area is bounded by 23.7856°N and 23.7714°N latitude and 90.6229°E and 90.6430°E longitude and part of a larger 25-km² area in Araihaazar upazila (sub-district), Bangladesh, where the ongoing *Health Effects of Arsenic Longitudinal Study* was launched in 2000 (Figure 1c; Ahsan et al., 2006). The site is located ~25 km east of the capital Dhaka and within the eastern perimeter of the expanding cone of depression induced by deep pumping (Khan et al., 2016; Knappett et al., 2016) (Figure 1). The occurrence of As in Araihaazar and the rest of the country has been shown to be largely geogenic (BGS/DPHE, 2001; Ravenscroft et al., 2009). Low-As aquifers are mainly associated with orange- or brown-colored, less reduced, Pleistocene sediment that outcrop in Dhaka City (Figures 1a and 1b); this area is known as the Madhupur Terrace (Morgan & McIntire, 1959). Beyond the city limits, however, low-As aquifers are generally overlain by more reduced Holocene gray sands commonly containing high dissolved As concentrations (Hoque et al., 2011; Horneman et al., 2004).

Table 1
Groundwater Physicochemical Parameters in Sand and Clay Formations

| Well ID | EC (μS/cm) | Depth (m) | Ca (mg/L) | Mg (mg/L) | Na (mg/L) | K (mg/L) | P (mg/L) | S (mg/L) | As (μg/L) | Fe (mg/L) | Mn (mg/L) | F (mg/L) | Cl (mg/L) | Br (mg/L) | DIC (mg/L) | DOC (mg/L) | δD (‰) | δ ¹⁸ O (‰) | |
|------------------------|------------|-----------|-----------|-----------|-----------|----------|----------|----------|-----------|-----------|-----------|----------|-----------|-----------|------------|------------|--------|-----------------------|-------|
| Sand formations | | | | | | | | | | | | | | | | | | | |
| S0 | 7.1 | 396 | 24 | 51 | 17 | 29 | 4 | 1.5 | 0.0 | 175 | 9 | 0.7 | 0.8 | 19 | 0.0 | 66 | 1.5 | -2.6 | -13.6 |
| S1 | 7.2 | 459 | 50 | 27 | 12 | 73 | 1 | 0.2 | 0.1 | 1 | 2 | 0.7 | 0.5 | 35 | 0.2 | 28 | 2.0 | -5.1 | -34.1 |
| S2 | 6.9 | 532 | 59 | 41 | 19 | 21 | 3 | 1.1 | 0.1 | 41 | 11 | 0.8 | 0.3 | 8 | 0.0 | 71 | 2.5 | -3.2 | -20.0 |
| S3 | 6.6 | 457 | 65 | 33 | 14 | 47 | 2 | 0.2 | 0.0 | 5 | 0.6 | 0.7 | 0.4 | 9 | 0.0 | 70 | 1.1 | -4.2 | -25.7 |
| CW-S | 6.9 | 542 | 195 | 33 | 0.0 | 28 | 2 | 0.2 | 0.9 | 2 | 0.8 | 0.0 | 1.2 | 0 | 2.6 | 46 | 1.1 | | |
| SS0 | 7.2 | 470 | 20 | 50 | 19 | 19 | 3 | 0.8 | 1.0 | 56 | 6 | 1.1 | 0.7 | 17 | 1.7 | 59 | 0.8 | -2.2 | -12.9 |
| SS1 | 7.1 | 569 | 44 | 42 | 19 | 207 | 4 | 1.7 | 0.1 | 68 | 13 | 0.3 | 2.0 | 40 | 0.1 | 58 | 1.9 | -4.8 | -29.3 |
| SS2 | 7.0 | 556 | 50 | 37 | 15 | 62 | 1 | 0.1 | 0.0 | 0.2 | 0.2 | 1.2 | 2.5 | 35 | 0.1 | 66 | 0.5 | -5.0 | -30.6 |
| SS3 | 7.1 | 199 | 59 | 44 | 20 | 31 | 2 | 0.2 | 0.0 | 15 | 4 | 1.0 | 2.0 | 8 | 0.0 | 68 | 2.2 | -4.0 | -23.2 |
| SS4 | 7.0 | 572 | 72 | 40 | 13 | 57 | 2 | 0.1 | 0.0 | 1 | 0.4 | 0.4 | 2.7 | 7 | 0.1 | 63 | 1.2 | -4.3 | -26.3 |
| M1-1 | 7.0 | 418 | 18 | 47 | 15 | 14 | 3 | 1.6 | 0.0 | 197 | 10 | 0.5 | 0.2 | 10 | 0.0 | 58 | 1.5 | -2.8 | -13.9 |
| M1-4 | 6.8 | 610 | 41 | 33 | 15 | 50 | 3 | 1.2 | 0.0 | 80 | 10 | 0.0 | 0.4 | 14 | 0.1 | 119 | 4.2 | -4.4 | -27.5 |
| M1-4a | 7.4 | 632 | 51 | 67 | 20 | 20 | 3 | 1.0 | 0.1 | 352 | 11 | 0.1 | 0.4 | 25 | 0.1 | 85 | 3.8 | -2.7 | -19.8 |
| M1-5 | 6.7 | 529 | 61 | 63 | 24 | 14 | 2 | 0.1 | 0.1 | 0.5 | 0.2 | 0.6 | 0.5 | 15 | 0.0 | 96 | 1.4 | -2.3 | -13.3 |
| M1-6 | 6.8 | 610 | 65 | 63 | 23 | 14 | 2 | 0.1 | 0.0 | 3 | 0.5 | 0.4 | 0.6 | 9 | 0.0 | 94 | 1.3 | -2.4 | -13.3 |
| M-CW | 6.8 | 441 | 96 | 33 | 0.0 | 26 | 2 | 0.1 | 0.1 | 0.3 | 0.1 | 0.0 | 1.2 | 6 | | | | | |
| T1 | 6.8 | 513 | 10 | 53 | 14 | 17 | 4 | 3.1 | 0.0 | 95 | 10 | 0.2 | 0.3 | 22 | 0.0 | 64 | 2.4 | -2.7 | -14.6 |
| T2 | 6.8 | 488 | 20 | 39 | 17 | 26 | 2 | 1.1 | 0.8 | 29 | 16 | 1.2 | 0.1 | 15 | 0.0 | 74 | 2.6 | -2.7 | -18.0 |
| T3 | 6.7 | 516 | 52 | 39 | 25 | 23 | 3 | 1.6 | 0.0 | 75 | 4 | 0.0 | 0.7 | 11 | 0.0 | 80 | 4.0 | -2.8 | -16.0 |
| T4 | 6.8 | 470 | 62 | 38 | 25 | 17 | 2 | 0.0 | 0.0 | 2 | 0.4 | 1.4 | 0.5 | 17 | 0.0 | 65 | 1.3 | -2.7 | -15.4 |
| CW-T | 6.8 | 630 | 195 | 42 | 0.0 | 36 | 2 | 0.2 | 0.4 | 2 | 1 | 0.0 | 1.3 | 0 | 1.3 | 49 | 1.9 | | |
| R0 | 7.2 | 301 | 34 | 26 | 6 | 10 | 2 | 1.5 | 0.0 | 163 | 2 | 0.6 | 0.9 | 5 | 0.0 | 29 | 0.5 | -3.6 | -20.0 |
| R1 | 7.2 | 330 | 51 | 27 | 13 | 13 | 3 | 0.5 | 1.5 | 23 | 6 | 1.2 | 0.2 | 8 | 0.0 | 32 | 0.5 | -3.1 | -18.4 |
| R2 | 7.2 | 325 | 66 | 27 | 20 | 12 | 3 | 0.2 | 0.0 | 1 | 1 | 0.2 | 0.6 | 5 | 0.0 | 36 | 0.5 | -3.3 | -17.9 |
| N0 | 7.1 | 822 | 32 | 65 | 28 | 28 | 5 | 2.6 | 0.1 | 110 | 10 | 0.2 | 1.1 | 36 | 0.7 | | | | |
| N1 | 7.1 | 540 | 47 | 34 | 20 | 51 | 3 | 0.9 | 0.0 | 15 | 8 | 0.1 | 0.2 | 10 | 0.1 | 65 | 1.7 | -4.9 | -32.2 |
| N2 | 7.1 | 449 | 63 | 22 | 8 | 73 | 2 | 0.2 | 0.0 | 5 | 2 | 0.3 | 0.3 | 13 | 0.1 | 59 | 1.0 | -3.7 | -27.3 |
| N3 | 6.8 | 417 | 195 | | | | | | | | | | | | | 49 | 1.4 | | |
| O1 | 7.2 | 506 | 56 | 41 | 21 | 20 | 2 | 0.8 | 0.0 | 55 | 9 | 0.0 | 0.3 | 16 | 0.0 | 53 | 1.4 | -3.2 | -20.1 |
| Q1 | 7.3 | 575 | 52 | 45 | 24 | 32 | 2 | 0.8 | 0.0 | 107 | 6 | 0.0 | 0.3 | 14 | 0.1 | 56 | 1.6 | -5.3 | -32.6 |
| Q2 | 7.3 | 625 | 58 | 35 | 17 | 86 | 2 | 0.6 | 0.2 | 39 | 7 | 0.6 | 0.3 | 12 | 0.1 | 74 | 0.8 | -5.3 | -32.9 |
| W-1 | 7.3 | 360 | 27 | 39 | 9 | 14 | 2 | 1.1 | 0.0 | 81 | 5 | 0.9 | 0.7 | 11 | 0.6 | 45 | 0.7 | -2.9 | -17.7 |
| W-2 | 7.2 | 687 | 43 | 56 | 31 | 287 | 6 | 1.8 | 0.0 | 171 | 8 | 0.1 | 1.5 | 33 | 0.0 | 96 | 3.0 | -5.0 | -30.5 |
| W-3 | 7.1 | 481 | 60 | 39 | 14 | 47 | 1 | 0.2 | 0.1 | 1 | 2 | 0.9 | 2.8 | 8 | 0.0 | 72 | 0.6 | -4.9 | -29.6 |
| W-4 | 7.0 | 483 | 67 | 24 | 9 | 234 | 1 | 0.2 | 0.1 | 8 | 3 | 0.3 | 1.7 | 8 | 0.4 | 53 | 0.6 | -4.6 | -27.3 |
| D1 | 6.9 | 403 | 20 | 38 | 0.0 | 15 | 4 | 1.7 | 0.1 | 166 | 17 | 0.0 | 0.8 | 18 | 0.2 | 52 | 1.7 | | |
| D2 | 6.8 | 1,393 | 59 | 32 | 0.0 | 332 | 2 | 0.2 | 0.3 | 5 | 2 | 0.0 | | 0 | 1.2 | 51 | 0.8 | | |
| J1 | 6.8 | 514 | 24 | 35 | 0.0 | 12 | 3 | 1.4 | 0.3 | 93 | 9 | 0.0 | 0.7 | 14 | 0.8 | 51 | 2.4 | | |
| J2 | 6.6 | 662 | 59 | 33 | 0.0 | 43 | 2 | 0.1 | 0.3 | 10 | 0.5 | 0.0 | 1.1 | 11 | 0.7 | 80 | 3.1 | | |
| L1 | 7.1 | 413 | 31 | 28 | 0.0 | 12 | 5 | 1.9 | 0.1 | 48 | 9 | 0.0 | 0.6 | 10 | 0.1 | 40 | 1.5 | | |
| L2 | 7.3 | 750 | 62 | 5 | 0.0 | 322 | 1 | 0.4 | 0.5 | 2 | 0.3 | 0.0 | 5.6 | 32 | 1.7 | 76 | 0.1 | | |
| B3 | 7.3 | 700 | 14 | 78 | 24 | 25 | 4 | 1.3 | 2.3 | 420 | 8 | 0.9 | | | | | | | |
| B4 | 7.2 | 1,022 | 28 | 87 | 28 | 29 | 4 | 1.4 | 0.0 | 218 | 11 | 0.2 | | | | | | | |
| B5 | 7.3 | 954 | 40 | 58 | 48 | 28 | 5 | 1.3 | 0.0 | 99 | 8 | 0.0 | | | | | | | |
| B6 | 7.4 | 548 | 53 | 32 | 23 | 83 | 2 | 0.3 | 0.0 | 12 | 3 | 0.3 | | | | | | | |
| B7 | 7.0 | 988 | 8 | 128 | 0.1 | 247 | 8 | 1.7 | 30.5 | 16 | 13 | 0.0 | | | | | | | |
| B8 | 7.0 | 704 | 11 | 92 | 0.0 | 58 | 5 | 2.0 | 10.5 | 212 | 13 | 0.0 | | | | | | | |
| B9 | 7.4 | 866 | 20 | 86 | 0.0 | 27 | 4 | 1.2 | 0.0 | 433 | 18 | 0.0 | | | | | | | |
| B-CW | 7.0 | 301 | 88 | 35 | 0.0 | 27 | 2 | 0.1 | 0.0 | 0 | 1 | 0.0 | 0.9 | 23 | 0.1 | | | | |
| CW-3 | | | 60 | 44 | 0.0 | 50 | 3 | 0.1 | 0.0 | 2 | 0.3 | 0.0 | 1.7 | 10 | 0.0 | | | | |
| Clay formations | | | | | | | | | | | | | | | | | | | |
| S | | 3 | | 33 | 19 | 18 | | 0.5 | 4 | 26 | 3 | 1.0 | 0.2 | 11 | 2.6 | | 24 | -3.2 | -22.1 |
| S | | 5 | | 50 | 38 | 17 | | 0.1 | 1 | 29 | 1 | 0.4 | 0.2 | 6 | 0.6 | | 11 | -3.9 | -24.2 |
| S | | 26 | | 41 | 24 | 38 | | 0.0 | 1 | 85 | 0.1 | 0.2 | 0.4 | 11 | 0.9 | | 7 | -2.7 | -17.3 |
| S | | 31 | | 18 | 27 | 58 | | 0.3 | 1 | 70 | 1 | 0.1 | 0.4 | 10 | 0.6 | | 12 | -3.5 | -21.7 |
| S | | 34 | | 11 | 5 | 77 | | 0.0 | 2 | 22 | 0 | 0.1 | 4.7 | 22 | 0.4 | | 30 | -3.0 | -19.1 |
| S | | 35 | | 18 | 7 | 89 | | 0.0 | 2 | 19 | 0 | 0.1 | 3.7 | 24 | 0.9 | | 14 | -2.7 | -18.2 |
| S | | 38 | | 22 | 8 | 90 | | 0.0 | 1 | 30 | 0 | 0.4 | 1.6 | 19 | 1.3 | | 14 | -2.1 | -14.8 |

Table 1
Continued

| Well ID | EC pH ($\mu\text{S}/\text{cm}$) | Depth (m) | Ca (mg/L) | Mg (mg/L) | Na (mg/L) | K (mg/L) | P (mg/L) | S (mg/L) | As ($\mu\text{g}/\text{L}$) | Fe (mg/L) | Mn (mg/L) | F (mg/L) | Cl (mg/L) | Br (mg/L) | DIC (mg/L) | DOC (mg/L) | δD (‰) | $\delta^{18}\text{O}$ (‰) |
|---------|-----------------------------------|-----------|-----------|-----------|-----------|----------|----------|----------|-------------------------------|-----------|-----------|----------|-----------|-----------|------------|------------|----------------------|---------------------------|
| S | | 40 | 15 | 8 | 99 | | 0.0 | 2 | 14 | 0.1 | 0.4 | | | | | 10 | -3.3 | -21.0 |
| S | | 41 | 15 | 7 | 87 | | 0.0 | 2 | 13 | 0 | 0.4 | | | | | 30 | -2.8 | -18.1 |
| M | | 2 | 466 | 232 | 321 | | 0.6 | 261 | 8 | 0 | 0.2 | 0.1 | 292 | 0.0 | | 21 | -2.6 | -14.3 |
| M | | 3 | 90 | 43 | 76 | | 0.0 | 20 | 1 | 0 | 0.1 | 0.2 | 39 | 16.4 | | 9 | -2.3 | -10.8 |
| M | | 5 | 76 | 48 | 43 | | 0.5 | 6 | 29 | 6 | 1.4 | 0.3 | 21 | 4.6 | | 11 | -2.8 | -15.3 |
| M | | 6 | 76 | 40 | 36 | | 0.4 | 1 | 49 | 4 | 1.9 | | | | | 5 | -2.5 | -13.5 |
| M | | 8 | 61 | 26 | 34 | | 2.0 | 2 | 54 | 5 | 0.6 | 0.3 | 12 | 1.2 | | 24 | -2.3 | -11.3 |
| M | | 9 | 57 | 23 | 57 | | 2.7 | 1 | 111 | 4 | 0.2 | 0.4 | 14 | 0.6 | | 21 | -2.3 | -10.5 |
| M | | 27 | 58 | 21 | 22 | | 0.5 | 1 | 190 | 2 | 0.2 | 0.5 | 10 | 0.9 | | 10 | -3.6 | -21.2 |
| M | | 29 | 60 | 21 | 39 | | 0.8 | 2 | 138 | 3 | 0.2 | | | | | 43 | -4.2 | -24.8 |
| M | | 31 | 51 | 17 | 49 | | 1.8 | 1 | 149 | 4 | 0.2 | 0.3 | 6 | 0.6 | | 49 | -3.9 | -25.5 |
| M | | 32 | | | | | | | | | | 0.4 | 8 | 1.0 | | | -4.5 | -28.1 |
| M | | 37 | | | | | | | | | | | | | | | | 25 |
| M | | 38 | | | | | | | | | | | | | | | | 17 |
| M | | 40 | | | | | | | | | | | | | | | | 29 |

Note. The median value is reported where long-term monitoring data are available.

The top of the Pleistocene aquifer was weathered (oxidized) during the last glacial maximum (20 ka BP) when the sediment was subaerially exposed and flushed by meteoric water as the sea level was at least 100 m lower than present day (Umitsu, 1994). In the northwestern portion of Araihasar, the oxidized, orange sand aquifer outcrops as the Madhupur Terrace. In the eastern and southeastern portion of Araihasar, this formation is buried under organic carbon-rich recent floodplain sediments of the Meghna and old Brahmaputra river system. Valley fill, channel migration, and avulsion of rivers and their distributaries (Morgan & McIntire, 1959; Pickering et al., 2014; Weinman et al., 2008) over the course of geologic time have partially eroded the sediments in the study area and resulted in the patchy occurrence of orange, oxidized deposits at variable depths further away from the uplifted Madhupur Terrace (Figure 1). Due to increasing utilization of the low-As intermediate (40- to 90-m depth) aquifer in Araihasar for water supply, the number of private wells tapping these Pleistocene orange sands quadrupled between 2001 and 2018 (supporting information Figure S1).

3. Methods

3.1. Monitoring Well Nests

3.1.1. Drilling and Installation

In addition to 15 previously described monitoring wells in the study area (Dhar et al., 2008; Horneman et al., 2004; Mihajlov, 2014; Stute et al., 2007; Zheng et al., 2005), 32 new monitoring wells at 10 nests (each nest consists of two to five monitoring wells) were installed between June 2012 and January 2017 (Figure 2b and Table 1). The new monitoring wells at Sites T, S, SS, N, Q, R, W, J, L, and D were installed to depths ranging from 9 to 195 m below ground surface (bgs) (Mozumder, 2019). The manual percussion (“hand flapper”) drilling technique (Horneman et al., 2004) was employed to install the shallow (<40 m bgs) and intermediate (>40–80 m bgs) wells with a 1.5-m screened interval at the bottom. Both sand and clay drill cuttings retrieved at regular intervals of 1.5 m were preserved for sediment analysis. In addition to four existing deep wells (>80 m bgs; Mihajlov et al., 2016) in the study area, three more deep wells were installed by the rotary drilling direct circulation (“donkey-pump”) method with a screened interval of 6 m. The depths of all installed wells were verified with a graduated water-level tape. Each monitoring well was constructed with a 5-cm-diameter stainless steel casing erected above the ground surface, followed by a series of connected 5- to 6-m-long PVC pipes that extended to the screened interval.

3.1.2. Water Level Monitoring

Hydraulic heads were monitored in 52 piezometers distributed across the study area. Hydraulic heads were measured manually with a water-level meter (Solinst Model 101 P2 probe) from the top of the

casing (TOC) of each monitoring well at regular intervals (on the third week of each month) between 2012 and 2018. The relative elevations of the TOC of each well were surveyed within ± 2 -cm accuracy based on closure using a 150-m-long transparent tube filled with water. All relative water level elevations were then converted to absolute water level elevations (i.e., elevation above mean sea level) with respect to Site B piezometers (Figure 2b), for which absolute elevation was determined in 2003 using a differential Global Positioning System (GPS) survey with a precision of ± 3 cm (Zheng et al., 2005). Automatic pressure transducers (Model 3001, Levellogger Edge, Solinst Canada Ltd., Georgetown, Ontario, Canada) were used in a subset of 25 monitoring wells to record water level in the wells more frequently. Barologgers (Barologger Edge, Solinst, Georgetown, Canada) were used to record atmospheric pressure at two well locations that were subtracted from water pressure measurements to obtain water level. All transducers were set to take synchronous measurements every 20 min. The automated water level measurements were compared with manual water level measurements to verify their accuracy over the duration of the deployments.

3.1.3. Onsite Chemical Measurements and Water Sampling

Before taking a sample from a monitoring well, at least one well-bore volume was purged with a submersible pump (Typhoon P-10200). This took 10 to 50 min depending on well depth. Groundwater samples were collected from sand aquifers in 2012–2017 after groundwater pH, oxidation-reduction potential (ORP), temperature, and electrical conductivity (EC) readings measured in a flow-through cell had stabilized (Oakton probes, UX-35650-10 and UX-35634-30). Pore-water samples were collected from clay layers by squeezing at Sites S and M in February 2016 using a mechanical squeezer (Manheim, 1966).

Polyethylene liquid scintillation vials (20-ml Wheaton Fisher 986706) with PolySeal caps were used to collect groundwater for cation, anion, and trace element analyses. Groundwater samples for stable water isotope (^2H and ^{18}O) analyses were collected in 20-ml scintillation glass vials with urea PolySeal caps (Wheaton Fisher 986546) in February 2016 and January 2017. Samples for tritium (^3H) were collected in 500-ml Amber Boston round bottles (Qorpak GLA00896) with a polycone lined cap (Qorpak 00190) in June 2012, May 2016, and Feb 2017. A subset of six wells from nest T, R, and S was sampled in duplicate in January 2018 for noble gas analyses (helium, He and neon, Ne) in crimped copper tubes (0.3" diameter, 30" length weighing approximately 40 cm^3 of water) following a prescribed protocol (<https://water.usgs.gov/lab/3h3he/sampling/>).

Samples for dissolved organic carbon (DOC) and dissolved inorganic carbon (DIC) analyses were collected in 22-ml clear glass vials (Sigma-Aldrich 27173 Supelco) with PTFE/silicone septum and screw caps (Sigma-Aldrich 27021 Supelco) in February 2016 and January 2017. The DOC samples were acidified to 0.1% HCl in the field immediately after collection. DIC vials were filled without leaving a headspace and not acidified. For radiocarbon dating of DIC and DOC, groundwater samples were collected in 250-ml bottles (Qorpak™ GLA00815) with a PolyCone Lined Cap. The DIC radiocarbon samples were preserved with 0.02% HgCl_2 and the radiocarbon DOC samples with 0.1% HCl.

To determine methane (CH_4) concentrations in groundwater, 60-ml groundwater samples collected with a syringe were injected through septa into pre-evacuated, burnt serum glass bottles fixed with Hg_2Cl and shipped upside-down for laboratory methane analyses of Sites SS, M, and B nest samples in January 2017 and Sites T, R, S, N, Q, D, J, and L nest samples in January 2018. Measurement of the stable carbon and hydrogen isotope ratios of CH_4 was performed on a subset of groundwater samples.

3.1.4. Groundwater Analysis

Concentrations of major cations and redox-sensitive trace elements Na, K, Ca, Mg, P, Fe, Mn, Sr, and Ba were measured by high-resolution inductively coupled plasma-mass spectrometry (HR ICP-MS) in groundwater acidified to 1% Optima grade HCl in the laboratory at least 1 week ahead of time (Cheng et al., 2004; van Geen et al., 2007). In the case of As, the precision was on the order of 5% and the detection limit based on the variability of the blank was $<0.1\ \mu\text{g/L}$. Base cations were measured with a precision of $\pm 10\%$ based on a laboratory and NIST-traceable standard. Concentrations of the major groundwater anions Br, F, and Cl were measured using a High Performance Ion Chromatography System (HPIC) (Dionex Integriion, Thermo Scientific) with an AS-18 column. This system has a detection limit of 0.05 mg/L and a precision of $\pm 5\%$ at environmental concentrations. Elemental concentrations reported in Table 1 indicate the median when time-series data are available.

Stable isotopes of ^{18}O and ^2H were analyzed with a Picarro Isotopic Water Analyzer at Lamont-Doherty Earth Observatory (LDEO) with a precision of $\pm 0.002\text{--}0.065\text{‰}$ for ^{18}O and $\pm 0.03\text{--}0.71\text{‰}$ for ^2H (Table 1). Working standards for the Picarro were stored in stainless steel casks under argon and measured yearly against the primary standards VSMOW2, GISP, and SLAP provided by IAEA in Vienna. An aliquot of an independent standard (not used for normalization) was run with each set of samples. Repeatability of ocean water measurements was $\pm 0.03\text{--}0.05\text{‰}$ (Walker et al., 2016).

Samples for tritium (^3H) were analyzed using the ^3He ingrowth technique from the decay of ^3H (Bayer et al., 1989; Ludin et al., 1998). The analytical precision for ^3H measurements was $\pm 0.01\text{--}0.1$ TU with a detection limit of 0.05–0.10 TU, where 1 TU corresponds to one ^3H atom per 10^{18} ^1H atoms. Two internal tritium standards had reproducibility of 1.1–1.5% (for ~8-TU tap water) and <50% (for ~0.12-TU ocean water). Noble gas concentrations and $^3\text{He}/^4\text{He}$ ratio were determined by mass spectrometry (Ludin et al., 1998; Stute et al., 2007) with a precision of $\pm 0.05\text{--}0.10\%$ for ^4He and Ne concentrations and $\pm 0.3\text{--}0.5\%$ for $^3\text{He}/^4\text{He}$ ratios. Long-term reproducibility of air equilibrated water samples for ^4He was 0.3–0.7%, for Ne was 0.3–0.8%, and for $^3\text{He}/^4\text{He}$ was 0.3–0.5%.

Both the DOC ($n = 30$) and DIC samples ($n = 45$) were analyzed in triplicate (three injections for each sample) on a Shimadzu Carbon Analyzer with a precision of $\pm 5\%$ at LDEO. Groundwater methane (CH_4) concentrations were measured at McMaster University by injecting 50–1,000 μl of headspace from the bottles using a SRI 8610C gas-chromatographer with a 0.91 m by 2.1 mm of silica gel column coupled to a flame ionization detector. Measurements were made in triplicate (RSD $\leq 10\%$) to compare with the calibration curves. PeakSimple Chromatography Software 3.29 (SRI Instruments) was used for peak analyses and integrations. Analyses of $\delta^{13}\text{C}$ and ^2H of CH_4 were performed by a GC-IRMS (Agilent 6890), also at McMaster University (Whaley-Martin, 2017).

3.2. Analysis of Sediment Cuttings

Drill cuttings (primarily sand and silt/clay) were wrapped with transparent plastic food wrap upon retrieval. A Konica Minolta CM-600d spectrophotometer was used to measure the difference in diffuse spectral reflectance between 530 and 520 nm (Horneman et al., 2004) through the plastic wrap soon after the samples were collected. Measurements were made in triplicate by the spectrophotometer and recorded for three different spots on each cuttings sample. Magnetic susceptibility of the sediment cuttings was measured at LDEO with a magnetic susceptibility meter (Model MS2, Bartington instrument, Oxford, England). A handheld X-ray fluorescence analyzer (InnovX Delta) was used in the three-beam soil mode to determine bulk As, Fe, and Ca concentrations in the sediment cuttings. Reference NIST standards SRM 2709, 2710, and 2711 were also analyzed by XRF at least at the beginning and end of each run to check calibration. Analysis of a subset of powdered sand samples ($n = 19$) from one of the sites by XRF confirmed that grain size did not affect the bulk concentrations.

A total of 45 pulverized, oven-dried drill cuttings of clay and occasionally encountered peat/charcoal layers from six sites collected from 3- to 73-m depth range were prepared for total carbon (TC) and inorganic carbon (IC) analyses. The samples were analyzed on the solid sample module (SSM) of Shimadzu Carbon Analyzer (TOC-Vcsn) by dry combustion at 900°C in the TC furnace and at 200°C in the IC furnace after acidifying the sample. The difference between the TC and IC was reported as total organic carbon (TOC). A subset of 20 drill cuttings from clay, peat, or buried wood fragments retrieved between 32- and 74-m depth interval at nine locations was sent to NOSAMS for radiocarbon dating of organic carbon (Elder et al., 1998). A subset of four clay cuttings was sent to the Particle Technology Lab (Downers Grove, IL) for porosity determination using the mercury intrusion method (Diamond, 1970) on an AutoPore IV 9500.

3.3. Pumping Tests

Two pumping tests were performed at Site M (Figure 2b). The first test was performed by pumping from the fully penetrating pumping well “M_A” (Site M, Well A) in the shallow aquifer for approximately 24 hr (17–18 January 2011). The second test was performed by pumping the entire vertical extent of the intermediate aquifer from the fully penetrating pumping Well B (M_B) for approximately 48 hr (19–21 January 2011). A locally purchased irrigation pump (1.75 horsepower, 1-atm maximum lift) was powered by a generator to maintain a constant flow rate of ~200 L/min (58 m^3/day), measured by a flow meter (McMaster-Carr) connected in-line to a PVC tube carrying the pump outflow.

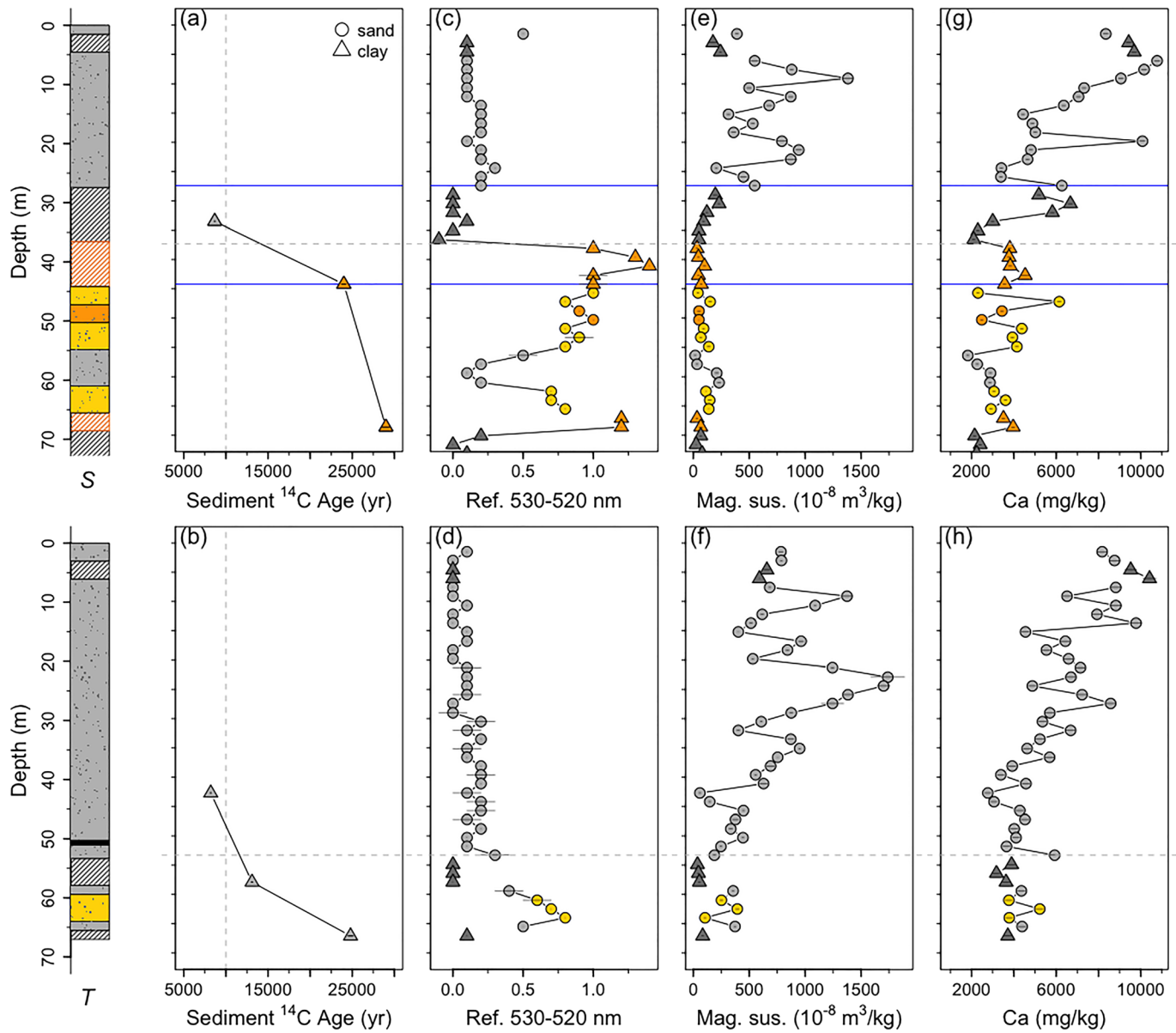


Figure 3. Sediment chemistry distinguishing Holocene from Pleistocene deposits. Depth profiles of sediment age (a and b), diffuse spectral reflectance (c and d), sediment magnetic mineral content (e and f), and calcium concentrations (g and h) for the clay-capped Site S (top panel) and sandy Site T (bottom panel) in the study area. The dotted horizontal gray lines indicate variations to the depth to the Pleistocene aquifer based on sediment radiocarbon dating. Typically, the Holocene sediment is gray whereas oxidized Pleistocene sediment is yellowish to orange in color (as shown in the accompanying borelogs). The sand facies is “dotted,” and the clay facies is “hatched.” The black thin band at Site T indicates a peat layer. The blue lines at Site S indicate the extent (or thickness) of the major clay aquitard capping the intermediate aquifer.

Hydraulic heads in multi-level observation wells and pumping Well C were monitored simultaneously by Solinst pressure loggers at 2-s intervals for the first 70 min of the tests, and at 1-min intervals for the remainder of the pumping tests and a 24-hr recovery period after pumping ended. A barometric pressure logger recorded atmospheric pressure changes on site at the same time intervals and was used to correct the pressure readings from the submerged loggers as explained in section 3.1.2. Several pressure loggers were deployed for weeks prior to and after the pumping tests to monitor the seasonally declining hydraulic head trend and atmospheric pressure changes.

3.4. Groundwater Flow and Solute Transport Modeling

A small-scale (3 km^2) MODFLOW (Harbaugh, 2005) based steady-state groundwater flow model was constructed using the USGS graphical user interface ModelMuse (Winston, 2019) on the basis of local stratigraphy. Both pumping and prepumping simulations were carried out on the basis of the homogeneous case of the large-scale ($11,025 \text{ km}^2$) transient model of Khan et al. (2016) (Figure 1), which was developed by refining the basin-scale ($362,700 \text{ km}^2$) model of Michael and Voss (2008) around Dhaka using the MODFLOW local grid refinement package. Our small-scale model has a refined grid size of $50 \times 50 \text{ m}$ and cell thickness of 1 m. The model comprises 202 layers with 41 columns in the east-west direction and 29 rows in the north-south direction.

3.4.1. Flow Model Boundary and Initial Conditions

The modeled domain is located about 25 km east of the pumping center in Dhaka City (Figure 1). Recharge was specified along the top of the model with a spatially uniform rate of 0.5 m/yr. A drain was also specified along the model top to prevent heads from exceeding the land surface elevation. The specified rate (0.5 m/yr) of recharge is consistent with regional estimates (Khan et al., 2016; Michael & Voss, 2009; Shamsudduha et al., 2011; Stute et al., 2007) as well as estimates on the basis of $^3\text{H}/^3\text{He}$ ages of shallow groundwater in Araihasar, Bangladesh (Stute et al., 2007). To assess the impact of the upper boundary condition, a model with a top constant head boundary (the assumption made in Michael & Voss, 2008) was also run given that there is little spatial variation in shallow groundwater head in the study area (Figure S2). The simulated heads were comparable (within an average absolute difference of 0.05 m) whether a uniform recharge or a constant head was specified at the model top.

Regional deep hydraulic heads decrease toward Dhaka, resulting in primarily westward flow in the study area (Khan et al., 2016; Knappett et al., 2016). No-flow boundaries were, therefore, assigned to the north and south model sides. The general head boundary (GHB) package was used to set hydraulic boundaries on the east and west sides and the bottom of the model for both pumping and prepumping scenarios. GHB is implemented to overcome three challenges: (i) no natural boundary (e.g., river) is present in proximity to the study area; (ii) a prescribed-head boundary with an infinite source of water may not be suitable when local pumping is invoked; and (iii) the stratigraphy is well constrained only within the study area, and the heterogeneity outside the modeled domain is uncertain. Because knowledge of the regional flow system is well defined based on previous studies (e.g., Khan et al., 2016), the utilization of reference heads and conductance from the regional model helps justify the use of GHB. GHB allows groundwater flow into and out of the model domain as a head-dependent flux with a conductance that represents aquifer resistance to flow between the simulated domain and known distal reference head.

The reference heads for the GHB were taken by interpolating the coarsely gridded ($1 \text{ km} \times 1 \text{ km} \times 5 \text{ m}$) simulated heads from the 66 model layers of Khan et al. (2016) for the pumping and prepumping scenarios. Because flux through the GHB requires assumption of a constant gradient between the location of the boundary and the distal defined reference head, the reference hydraulic heads were extracted from the larger-scale model at the maximum distance from the edge of the model area across which the gradient is constant. For the pumping scenario, the distance of the reference heads from the east and west boundary cells of our model was 1 km. Beyond that distance, the reference heads declined nonlinearly in the west due to Dhaka pumping and plateaued in the east closer to the Meghna River (Figure S3). Similar simulated heads were obtained as we varied the distance to the reference heads within $\leq 1 \text{ km}$. The simulated heads were sensitive to the nonlinearly distributed reference heads at distances $>1 \text{ km}$. Likewise, the GHB at the bottom of the model was assigned at 200 m with the reference heads extracted from 300 m. The conductance was calculated at the sides of the model as $K_h A/L$ and at the bottom as $K_v A/L$, where A is the cross-sectional area perpendicular to flow direction, L is the distance (sediment thickness), and K_h and K_v are the horizontal and vertical hydraulic conductivity, respectively.

3.4.2. Heterogeneity

A three-dimensional (3-D) lithofacies model of the study area was generated in Rockware15 software (Rockworks™) by interpolating between 33 driller logs (Figure S4a) at 1-m vertical resolution and 50-m horizontal resolution (Figure S5). The model consists of two major lithofacies (sand and clay) compared to Khan et al.'s four lithofacies (fine to very fine sand, medium to coarse sand, silt, and clay). Heterogeneity was explicitly represented up to a depth of 75 m, and the rest (75–200 m) was kept homogenous but anisotropic

(Figure S6). The depth for the heterogeneous portion of the model corresponds to the maximum depth local drillers can reach with the hand-percussion technique. The cuttings retrieved by hand-percussion drilling make a reliable distinction between sand- and clay-sized particles up to a depth of 75 m, whereas the direct circulation technique (donkey drilling) usually produces unreliable mixed cuttings. A sensitivity analysis was performed by extending the 3-D model domain in all directions (with extrapolated lithofacies) beyond the focus area by 0.5–1 km. Extending the domain did not affect the simulated heads in the study area.

3.4.3. Domestic and Irrigation Pumping

The pumping scenario accounts for domestic and shallow irrigation withdrawals within the model domain. A total of 1,270 hand pumps and 37 irrigation wells were all assigned individually in the model (Figure 2a). The hand pumps were identified during a 2012–2013 blanket As testing campaign (van Geen et al., 2014), whereas the irrigation well locations in the study area were determined in 2014 (Figure 2a).

The depths of domestic hand pump wells ranged from 9 to 197 m, and a screened interval at the bottom of the wells of 2 m was assumed. The domestic demand was estimated based on usage of 10 L per person per day (Zheng et al., 2005) and a five-person household sharing each well, resulting in 50 L of withdrawal per well per day.

The depth of irrigation wells ranged from 15 to 26 m, with an average screened interval of 5 m. The pumping rate of the most popular low-cost 2-HP submersible irrigation pump (100 QRm 3/16 #85054) was determined by matching the name of the manufacturer of the pump in the local market. The maximum flow rate of 70 L/min indicated by the manufacturer was used to calculate the rate of irrigation pumping. Since irrigation pumps are active for 4 months/yr and each pump runs for half a day on average, based on conversations with local farmers, a pumping rate of about 17% of the maximum pumping rate (11.7 L/min) was spread over 24 hr of every day of the year for the steady-state model simulation.

3.4.4. Flow Model Calibration

The steady-state groundwater flow model was calibrated manually to average observed heads for the entire model domain (0–200 m) with an overall root mean squared error of about 0.5 m (Figure S7). In the heterogeneous portion (model top to 75 m bgs), the individual facies K values were adjusted for model calibration. During each adjustment, equivalent K_h and K_v values were determined numerically in the homogeneous portion of the model (75–200 m) by simulating Darcy's flux horizontally and vertically across the 75-m heterogeneous domain. The calibrated Ks are similar to that of Khan et al. (2016).

The calibrated K_h value for the sand facies is 2×10^{-4} m/s and 9×10^{-9} m/s for the clay facies. These are similar to the K_h values for the greater Dhaka region calibrated by Khan et al. (2016) for medium to coarse sand facies (5.7 to 7.7×10^{-4} m/s) and silt facies (3.9 to 4.4×10^{-9} m/s), respectively. The calibrated equivalent K_h of 1.5×10^{-4} m/s and K_v of 8×10^{-8} m/s ($K_h/K_v = 1,875$) are also similar to previous values of Khan et al. (2016) of equivalent K_h of 2×10^{-4} m/s and K_v of 1×10^{-7} m/s ($K_h/K_v = 1,818$), respectively. A consistent vertical anisotropy (K_h/K_v) of 100 was used for both sand and clay facies whereas Khan et al. (2016) used a K_h/K_v of 10 for medium to coarse sand, 100 for fine to very fine sand, and 1 for both the silt and clay facies groups.

The shallow simulated heads were slightly over-predicted (by ~ 0.4 m) but were spatially homogeneous throughout the study area, consistent with measurements. The simulated and measured hydraulic head distributions in the intermediate aquifer were similar, although there were some discrepancies. The difference in observed and simulated heads in 20 out of the 30 intermediate wells ranged between -0.49 and 0.44 m (absolute average error of 0.22 m), five with a discrepancy from -0.86 to 0.66 . Four out of the five wells with a higher average discrepancy of 1.3 m were located near the western boundary. The model under-prediction in that area was likely due to proximity to lower boundary heads and a lack of hydrostratigraphic data outside of the study area. The simulated deep aquifer heads were consistent with the westerly decreasing observed heads and flow direction in response to Dhaka pumping. The average difference between simulated and measured heads in the deep aquifer (100–195 m) was 0.27 m ($n = 5$). Differences in hydraulic heads among the observations ($n = 52$) and simulations in all aquifers are well within the seasonal fluctuations of groundwater level in the study area.

3.4.5. Arsenic Transport Modeling

Advective transport of As was simulated by particle tracking using MODPATH version 6 (Pollock, 2012) to estimate the travel time required for groundwater to travel from the recharge area into the intermediate

aquifer in the absence of retardation. Particles were tracked backward from five nests (Sites T, R, S, M, and B) in the intermediate aquifer (45–65 m) and were allowed to travel over a prescribed time interval of 100 yr for the pumping scenario and 500 yr for the prepumping scenario.

The MT3DMS package (Zheng & Wang, 1999) was used to simulate advective-dispersive transport of As in groundwater while accounting for adsorption (e.g., Michael & Khan, 2016). For simplicity, a constant (relative) concentration (C/C_0) of 1 was applied to the model top, and zero flux along the east and west boundaries. An initial concentration of 1 was applied to the shallow aquifer (0- to 30-m depth) and 0 was applied to the rest of the aquifer. In this case, retardation factors of 3, 10, and 30 were applied for all lithofacies assuming a linear isotherm to predict the three-dimensional distribution of As in the intermediate aquifer under different sorption scenarios (Figure S8). A partition coefficient, K_D of 1.5 L/kg translates into a retardation factor (R_f) of 10 when a porosity of 0.3 and bulk density of 1.8 g/cc are assumed. A constant longitudinal dispersivity value of 10 m and transverse dispersivities of 0.01 (horizontal) and 0.001 m (vertical) were assigned (Michael & Khan, 2016). Forward simulations were performed with and without the effect of pumping for 100 and 500 yr, respectively. A porosity of 0.3 was assumed for both MODPATH and MT3DMS simulations.

4. Results

4.1. Hydrostratigraphy

The shallow aquifer (30 m deep) in the study area consists of a fining-upward sequence of gray channel sands capped by surficial clay at 29 out of 33 drill sites (Figures 2a and S4a), below which groundwater As levels are generally elevated compared to deeper aquifers (Figure S1). A thick clay aquitard of variable thickness typically separates the shallow and intermediate aquifer in Araihasar, as it does in many regions of the Bengal basin. In our 3-km² study area, this aquitard is up to 24 m thick but almost entirely absent at drilling Sites R and T (Figures 2a and S4a). The top of this aquitard, where present, is generally encountered at 25- to 30-m depth (Figure S4a). The intermediate aquifer (>40–80 m) located below this aquitard is semi-confined. In most cases, depending on location, a second harder clay layer was encountered in the 65- to 80-m depth range and could not be penetrated with the local driller's hand-percussion method (Figure S4a). In this study, this hard clay layer is considered the bottom of the intermediate aquifer. Pumping test results within this semi-confined aquifer yielded an average K_h of 1×10^{-4} m/s and storativity (S) of 6.2×10^{-4} (Figure S9 and Table S1), which are typical for confined aquifers composed of medium- to fine-grained sands.

The shallow aquifer is primarily composed of gray sand whereas the intermediate aquifer shows inter-fingering of both gray and orange sand sequences (Figure S4a). The difference in sediment color was quantified by the difference in diffuse spectral reflectance ΔR between 530 and 520 nm (Horneman et al., 2004). The ΔR values recorded on a total of 461 sediment cuttings of gray sand and clay averaged $0.2 \pm 0.1\%$ and contrast with ΔR averaging $0.9 \pm 0.2\%$ ($n = 111$) for drill cuttings retrieved from the oxidized orange/reddish sand and clay sequences. At 24 of the 33 drill sites, the upper 1–24 m of the intermediate aquifer sand is gray (reduced) in color. For 12 out of 33 drill sites, there is also a gray sand layer in the intermediate aquifer that is sandwiched between orange (oxidized) sands at a depth that varies from one drill site to the other. At 5 of the 33 drill sites, the bottom of the clay layer capping the intermediate aquifer is oxidized, reddish brown in color, and has been described elsewhere as a paleosol (McArthur et al., 2004, 2008, 2011) that protects the low-As intermediate orange sand aquifer (Figure S4a).

The proportion of clay relative to sand within the upper 50 m at each drill site varies spatially from 3% to 73% (Figure 2a). At 5 of the 33 drill sites, the proportion of clay is $\leq 20\%$. These sandy sites, where the intermediate aquifer is directly connected to the shallow aquifer, are located on the periphery of the study area.

4.2. The Holocene-Pleistocene Transition

Oxidized orange sediments are generally considered of Pleistocene age across the Bengal Basin (Ahmed et al., 2004; McArthur et al., 2004). We refine this assessment in our study area on the basis of radiocarbon dating of clay or peat, profiles of magnetic susceptibility, and bulk concentrations of calcium (Ca) in sediment based on the cuttings (Figures 3a, 3b, and 3e–3h). Radiocarbon ages of 23 clay cuttings from between depths 32 and 78 m range from 6.5 to 36.5 kyr (Figure S4b). Overall, the data show the expected increase in age with depth, but also that the depth of the Holocene-Pleistocene boundary can vary significantly within a

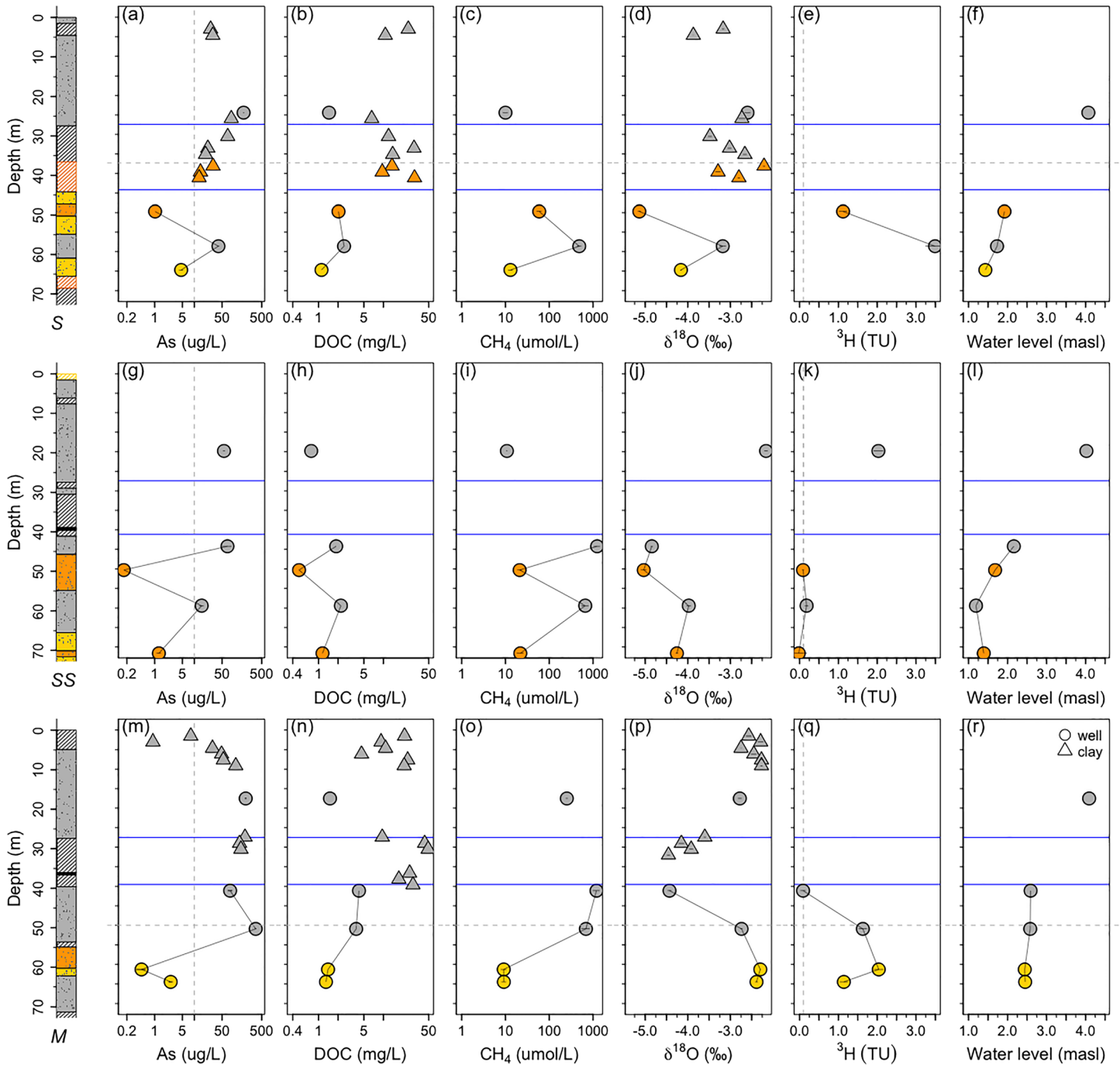


Figure 4. Groundwater hydrogeochemistry at three clay-capped sites. Depth profiles within sand aquifer and clay aquitard pore waters of dissolved arsenic (As) (a, g, and m), dissolved organic carbon (DOC) (b, h, and n), dissolved methane (CH_4) (c, i, and o), stable isotope of oxygen ($\delta^{18}\text{O}$) (d, j, and p), tritium (^3H) (e, k, and q), and average hydraulic head (f, l, and r) at Site S (well ID: S0, S1, S2, and S3), Site SS (well ID: SS0, SS1, SS2, SS3, and SS4), and Site M (well ID: M1–1, M1–4, M1–4a, M1–5, and M1–6), respectively. Concentrations of As, DOC, CH_4 , and $\delta^{18}\text{O}$ are provided in Tables 1 and 3. The highest measured ^3H concentrations are shown from Table 2. The blue lines indicate the extent (or thickness) of the major clay aquitard capping the intermediate aquifer. The dashed horizontal gray lines indicate the approximate Holocene to Pleistocene transitional depth based on radiocarbon age of sediment cuttings (see Figure S4b). The dashed vertical lines indicate the WHO guideline of $10 \mu\text{g/L}$ for As (a, g, and m) and detectable level (0.1 TU) of ^3H (e, k, and q). Note that the x-axes of As, DOC, and CH_4 are presented in log-scale.

Table 2
Groundwater ^3H Concentrations and Apparent $^3\text{H}/^3\text{He}$ Ages Estimated for a Subset of Samples

| Well ID | Depth (m) | $^3\text{H} \pm 1\sigma$ (TU) | | | | $^3\text{H}/^3\text{He}$ He age (yr) |
|-----------|-----------|-------------------------------|-------------|--------------|-------------|--------------------------------------|
| | | 2011 ^a | 2012 | 2017 | 2018 | |
| S1 | 49.7 | | | 1.12 ± 0.05 | 0.22 ± 0.04 | 45 ± 3 |
| S2 | 58.6 | | | | 3.49 ± 0.12 | 47 ± 1 |
| SS0 | 19.8 | | | 2.03 ± 0.06 | | |
| SS2 | 50.3 | | | 0.09 ± 0.01 | | |
| SS3 | 59.4 | | | 0.18 ± 0.02 | | |
| SS4 | 71.6 | | | −0.02 ± 0.10 | | |
| S-CW | 195.0 | | | 0.06 ± 0.04 | | |
| M1–4 | 41.1 | 0.09 ± 0.03 | | | | |
| M1–4a | 50.9 | 1.61 ± 0.05 | | 1.63 ± 0.05 | | |
| M1–5 | 61.3 | 2.04 ± 0.06 | | | | 39 ± 2 |
| M1–6 | 64.5 | 0.54 ± 0.03 | | 1.14 ± 0.05 | | 49 ± 1 |
| M2–5 | 60.1 | 1.22 ± 0.05 | | | | 27 |
| M2–6 | 68.6 | 0.13 ± 0.03 | | | | 40 ± 2 |
| M3–5 | 59.8 | 2.68 ± 0.06 | | | | 11 ± 0 |
| M3–6 | 67.4 | 1.21 ± 0.05 | | | | 25 ± 0 |
| M4–5 | 54.5 | 0.81 ± 0.04 | | | | 25 ± 3 |
| M4–6 | 63.5 | 0.08 ± 0.03 | | | | 69 ± 1 |
| T1 | 9.5 | | 2.78 ± 0.07 | | | |
| T2 | 20.1 | | 3.04 ± 0.08 | | | |
| T3 | 51.8 | | 1.88 ± 0.06 | 1.88 ± 0.06 | 1.83 ± 0.07 | 24 ± 1 |
| T4 | 62.3 | | 1.48 ± 0.06 | | 2.10 ± 0.08 | 14 ± 1 |
| T-CW | 195.0 | | | 0.07 ± 0.07 | | |
| T-CW- dup | 195.0 | | | 0.04 ± 0.06 | | |
| R1 | 50.7 | | | 2.64 ± 0.08 | 2.36 ± 0.09 | 40 ± 1 |
| R2 | 65.6 | | | 2.72 ± 0.07 | 2.64 ± 0.09 | 27 ± 1 |
| N0 | 32.0 | | | 1.17 ± 0.09 | | |
| N1 | 47.4 | | | −0.04 ± 0.02 | | |
| N2 | 63.0 | | | −0.06 ± 0.01 | | |
| Q1 | 52.2 | | | 0.08 ± 0.02 | | |
| Q2 | 58.0 | | | 0.06 ± 0.01 | | |
| W1 | 27.4 | | | 2.26 ± 0.06 | | |
| W2 | 42.7 | | | 0.05 ± 0.02 | | |
| W4 | 67.7 | | | 0.04 ± 0.02 | | |
| J1 | 25.0 | | | 1.96 ± 0.09 | | |
| J2 | 59.1 | | | 0.11 ± 0.07 | | |
| L1 | 30.5 | | | 2.14 ± 0.10 | | |
| L2 | 61.6 | | | 0.25 ± 0.10 | | |
| D2 | 59.4 | | | −0.02 ± 0.07 | | |
| O1 | 56.3 | | | 1.16 ± 0.04 | | |
| CW3 | 60 | | | −0.03 ± 0.03 | | |

^a After Mihajlov et al. (2020).

lateral distance of a few hundreds of meters. At scoured Site T near the southern boundary of the study area, which is representative of five other locations (Figure 2a), the confining clay layer is missing and Holocene gray sands extend all the way down to 53-m depth. At Site S, representative of 25 locations with a clay cap, the intermediate aquifer is capped by an oxidized, Pleistocene paleosol at a depth as shallow as 37 m (Figure 3).

Profiles of magnetic susceptibility and Ca help define the Holocene-Pleistocene transition at each site (Figures 3e and 3f). The contribution of magnetite and other magnetic minerals to Holocene sediments is variable but distinctly higher than for Pleistocene sediments (BGS/DPHE, 2001; Horneman et al., 2004). The bulk Ca content of Holocene sands is also higher than for Pleistocene intervals (Figures 3g and 3h). These differences have been attributed, respectively, to the partial reduction of Fe oxides forming magnetite and the authigenic precipitation of carbonate in supersaturated Holocene sediments (McArthur

Table 3
Methane and Its Isotopes in Groundwater of Araihasar, Bangladesh

| Well ID | Depth (m) | CH ₄ ($\pm 1\sigma$) ($\mu\text{mol/L}$) | $\delta^{13}\text{C}$ (‰) | δD (‰) |
|---------|-----------|---|---------------------------|----------------------|
| S0 | 24.4 | 10 \pm 1 | | |
| S1 | 49.7 | 59 \pm 4 | | |
| S2 | 58.6 | 484 \pm 24 | | |
| S3 | 64.7 | 13 \pm 1 | | |
| SS0 | 19.8 | 11 \pm 0.1 | −70.5 | |
| SS1 | 44.2 | 1,239 \pm 93 | −67.3 | |
| SS2 | 50.3 | 21 \pm 1 | −72.4 | |
| SS3 | 59.4 | 662 \pm 60 | −79.6 | |
| SS4 | 71.6 | 22 \pm 2 | −62.6 | |
| M1-1 | 17.5 | 252 \pm 5 | | |
| M1-4 | 41.1 | 1,199 \pm 100 | | |
| M1-4a | 50.9 | 688 \pm 70 | | |
| M1-5 | 61.3 | 9 \pm 1 | | |
| M1-6 | 64.5 | 9 \pm 1 | | |
| T1 | 9.5 | 63 ^a | | |
| T2 | 20.1 | 1 \pm 0.1 | | |
| T3 | 51.8 | 90 \pm 5 | | |
| T4 | 62.3 | 2 \pm 0.1 | | |
| R0 | 33.5 | 8 \pm 0.4 | | |
| R1 | 50.7 | 1 \pm 0.1 | | |
| R2 | 65.6 | 2 \pm 0.1 | | |
| N1 | 47.4 | 943 \pm 47 | | |
| Q1 | 52.2 | 25 \pm 1 | | |
| J2 | 59.1 | 44 \pm 2 | | |
| L2 | 61.6 | 10 \pm 1 | | |
| CW-B | 88 | 65 \pm 2 | −80.6 | −109.2 |
| B3 | 14.2 | 2.5 \pm 0.01 | | |
| B4 | 27.9 | 208 \pm 10 | −84.1 | −160.8 |
| B5 | 40.1 | 207 \pm 14 | −85.8 | −209.0 |
| B6 | 52.7 | 331 \pm 27 | −84.4 | −200.5 |
| B7 | 8.1 | 3 \pm 0.1 | | |
| B8 | 11.1 | 11 \pm 1 | | |
| B9 | 20.3 | 34 \pm 3 | | |

^aMeasured in the field using a GX-6000 IR Analyzer (RKI Instruments).

et al., 2008; van Geen et al., 2013). These authigenic phases evidently never formed or were not preserved during subaerial exposure of Pleistocene sediments during the most recent low stand in sea level about 20 kyr ago.

Unlike Ca, the solid phase As and Fe content of Holocene and Pleistocene sands are comparable. The average As concentrations of the Holocene gray and Pleistocene orange sands are 3 \pm 1 mg/kg ($n = 100$) and 2 \pm 1 mg/kg ($n = 21$), respectively, based on measurements from six sites drilled in the study area. Arsenic concentrations in clay are typically higher (up to 7–15 mg/kg) than in sand cuttings, but there is no noticeable difference between Holocene and Pleistocene clay. The bulk Fe concentration of Pleistocene (1.0 \pm 0.3%, $n = 21$) and Holocene gray sand (1.2 \pm 0.4%, $n = 100$) is similar.

The gray Holocene aquifer contains wood fragments and peat- or charcoal-like fragments in the study area (Figure S4a) of a type that has been dated extensively in other parts of the country (Goodbred & Kuehl, 2000). In our study area, a total of 16 buried peat/wood layers were discovered during drilling in 14 out of the 33 logs within the 6- to 52-m depth interval. The concentrations of total organic carbon (TOC) measured in seven such peat fragments from five locations ranged from 12% to 50% by weight with an average of 30 \pm 10%, contrasting with an average of about 0.5 \pm 0.2% (maximum of 3.1%) measured on 38 less dark clay cuttings retrieved from six locations in the study area. The TOC (%) for gray Holocene clay is systematically >0.1% whereas the orange Pleistocene clay sequences typically contain <0.1% organic carbon (Figure S10).

4.3. Groundwater Chemistry

4.3.1. Clay-Capped Portion of Intermediate Aquifer

Sites S and SS are two geologically comparable sites located 150 m apart in the center of the study area (Figure 2b). In this area, the intermediate aquifer is capped by a stiff, confining clay layer (Figures 4a–4l). At Site S, the top half of the confining clay layer is reduced, gray and of Holocene age and the bottom half is oxidized and of Pleistocene age (Figure 3a). The top and bottom sands of the Pleistocene aquifer are orange and low in groundwater As (<5 $\mu\text{g/L}$) whereas the reduced, gray middle of the aquifer is elevated in groundwater As (40 \pm 5 $\mu\text{g/L}$) (Figure 4a). This reduced portion of the aquifer with elevated As at Site S is also high in dissolved Fe (11 \pm 2 mg/L), P (1 \pm 0.5 mg/L), DOC (2.5 mg/L), CH₄ (484 \pm 24 $\mu\text{mol/L}$), and bomb-produced ³H (3.5 \pm 0.1 TU) compared to the oxidized portions of the aquifer above and below (Figures 4a–4c, 4e, S11a, and S11b and Tables 1–3). The composition of groundwater in reduced, gray sand is similar to that of shallow groundwater at this site (Figure 4d). The southward extension of the reduced portion of the intermediate aquifer at Site SS is less elevated in dissolved As (15 \pm 2 $\mu\text{g/L}$) with barely detectable (>0.1 TU) ³H, but DOC and CH₄ levels are comparable to those in the reduced portions of the intermediate aquifer at Site S (Figures 4g–i, 4k). In gray sand just below the clay layer at Site SS, both As and CH₄ concentrations are high at 70 $\mu\text{g/L}$ and 1,200 $\mu\text{mol/L}$, respectively. The CH₄ is depleted (<−58 \pm 5‰) in $\delta^{13}\text{C}$ (−63‰ to −86‰, $n = 9$) and $\delta^2\text{H}$ (−109‰ to −209‰, $n = 4$), which confirms its biogenic origin (Table 3) (Simpkins & Parkin, 1993).

Site M, located 450 m south of Site S (Figure 2b), has been studied extensively following the repeated failure (i.e., a rise in As) of a community well installed in the intermediate aquifer that served the neighboring villagers (Mihajlov et al., 2020; van Geen et al., 2006). Long-term monitoring of two wells at Site M, where the intermediate aquifer is capped by thick clay, indicates elevated levels of As (80 \pm 29 and 350 \pm 21 $\mu\text{g/L}$), Fe (10 \pm 2 and 11 \pm 1 mg/L), P (~1 \pm 0.1 mg/L), DOC (~4 mg/L), and CH₄ concentrations (1,200 \pm 100 and 690 \pm 70 $\mu\text{mol/L}$). In contrast, the wells installed in the oxidized, lower portion of the aquifer (>55 m) are low in As, Fe, P, and CH₄ (Figures 4m–4o, S11g, and S11h). Unlike at Site S, ³H was not detected in the

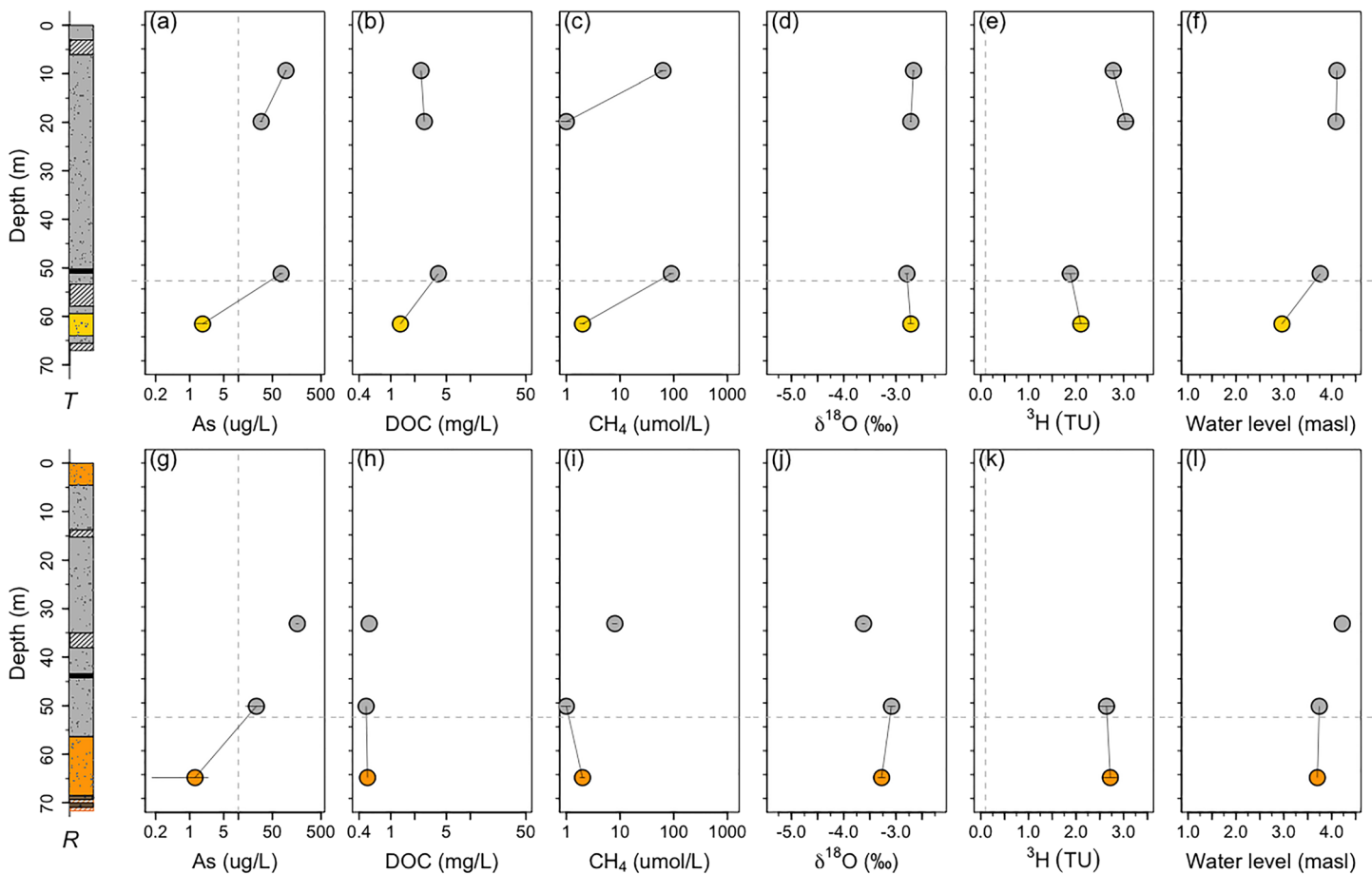


Figure 5. Groundwater hydrogeochemistry at two sandy sites. Depth profiles of groundwater arsenic (As) (a and g), dissolved organic carbon (DOC) (b and h), dissolved methane (CH_4) (c and i), stable isotope of oxygen ($\delta^{18}\text{O}$) (d and j), tritium (^3H) (e and k), and average hydraulic head (f and l) at the sandy Site T (well ID: T1, T2, T3, and T4) and Site R (well ID: R0, R1, and R2), respectively. See Figure 4 for the explanation of the dashed gray lines. The x-axes of As, DOC, and CH_4 are in log-scale.

well immediately below the confining clay layer (Figure 4q). The stable isotopic composition of groundwater in gray sand beneath the thick clay differs by 1.5‰ and 12.5‰ for ^{18}O and ^2H , respectively, from that of groundwater in the shallow aquifer above the clay (Figure 4p).

Pore waters extracted from clay at Sites S and M are elevated in dissolved As (maximum of 190 $\mu\text{g/L}$) and contain an order of magnitude higher DOC concentrations (maximum of 49 mg/L with an average of 20 ± 5 mg/L) compared to groundwater in the intermediate aquifer (Figures 4a, 4b, 4m, and 4n). The stable isotopic composition of clay pore water in both gray and orange clay at Site S is comparable to that of the shallow aquifer (Figure 4d). Groundwater just below the orange clay is more depleted in ^{18}O by about 2‰ at this site. In contrast, the stable isotope composition of gray clay water at Site M is similar to that of groundwater in gray sand just below the clay (Figure 4p). At both sites, high concentrations of conservative elements (e.g., Na and Br) were detected in the clay and the intermediate aquifer directly beneath it (Figures S11c, S11f, S11i, and S11l).

The ages of groundwater containing detectable ^3H (>0.1 TU) in the intermediate aquifer range from 11 to 49 yr at Site M ($n = 9$) and 45 to 47 yr at Site S ($n = 2$) (Table 2). With the exception of Wells S2 and M3.5, the $^3\text{H} + ^3\text{He}$ content of these samples, which is unaffected by ^3H decay, accounts for $<70\%$ of the predicted value based on a smoothed version of ^3H input to groundwater since 1950 (Figure S12), indicating that most of these samples are mixtures of old groundwater recharged before bomb- ^3H input with younger groundwater containing bomb- ^3H .

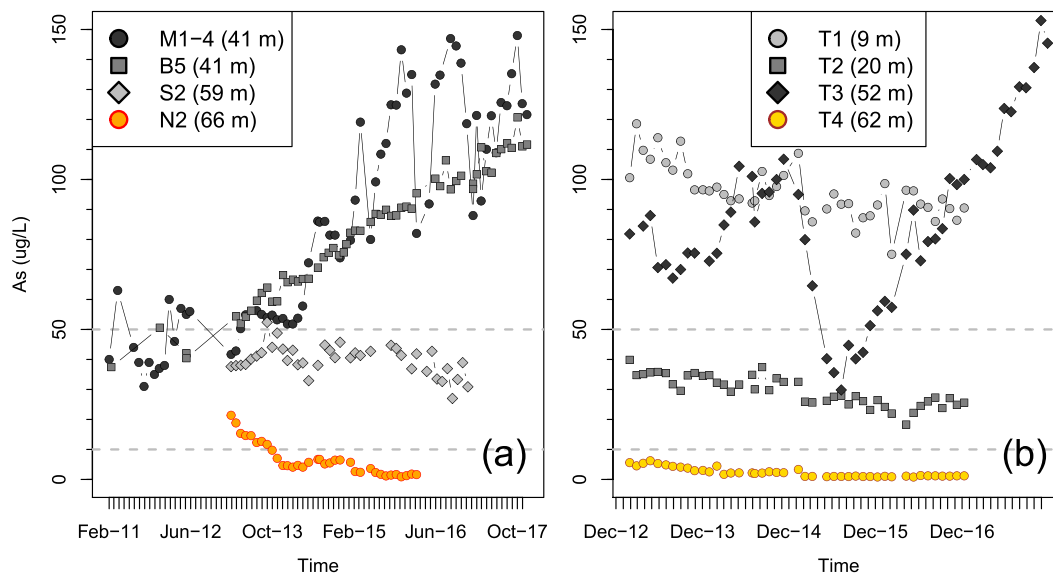


Figure 6. Evolution of As concentrations in the intermediate aquifer. (a) Increase (B5 and M1–4), decrease (N2), and stable (S2) As concentrations in four wells in the confined aquifer. (b) Examples of cyclic rise and fall (T3) and steady decline (T1, T2, and T4) in As concentrations in a sandy site.

4.3.2. Portion of Intermediate Aquifer Without a Clay Cap

The composition of groundwater as a function of depth at the two sandy Sites R and T, 700 m to the west and 750 m to the south of Site M, is somewhat featureless compared to Sites SS, S, and M (Figures 2 and 5). The gray sandy aquifer at Sites R and T is elevated in dissolved As ($>50 \mu\text{g/L}$) to a depth of 55 m (Figures 5a and 5g). At greater depth, groundwater in contact with orange Pleistocene sands contains $<5 \mu\text{g/L}$ of As. The DOC concentrations at Site T are relatively high (highest at 4 mg/L in an intermediate well installed immediately below a peat layer) whereas all monitoring wells at Site R are consistently low (0.5 mg/L) in DOC (Figures 5b and 5h). Methane concentrations in groundwater at the sandy sites are lower than that in the gray sand layers where the intermediate aquifer is capped by clay, by a factor of 10 and 100 at Sites T and R, respectively (Figures 5c and 5i).

The stable isotope compositions of groundwater in the shallow and intermediate aquifer at sandy Sites R and T, including orange sands at depth, are similar to those of the shallow aquifer (Figures 5d and 5j). Bomb-produced ^3H also penetrates the intermediate aquifers to the depth of orange sand at all sandy sites (Figures 5e and 5k). The estimated age of groundwater in the intermediate aquifer based on the $^3\text{H}/^3\text{He}$ method at Sites T and R ranges from 14 to 24 yr and 22 to 38 yr, respectively (Table 2). The distribution of $^3\text{H}+^3\text{He}$ relative to predicted bomb input show no indication of mixing of young and old groundwater in these samples, unlike the ^3H -containing samples from the portion of the intermediate aquifer capped by clay (Figure S12).

4.3.3. Long-Term Changes in As Concentrations in the Intermediate Aquifer

Two intermediate wells at clay-capped Sites M and B monitored for more than 5 yr indicate a steady increase in As concentrations, a third well at Site S shows steady As levels, while fourth at Site N indicates a slight decline in As (Figure 6a). Both wells with rising As were installed beneath the gray confining clay layer, at the same depth of 41 m. Well M1–4 (41 m) at the clay-capped Site M, which is devoid of ^3H and has a similar isotopic and conservative solute composition to that of overlying clay pore-water (Mihajlov et al., 2020) (Figures 4p, S11i, and S11k), shows a steady increase in As from $40 \mu\text{g/L}$ in February 2011 to $150 \mu\text{g/L}$ in October 2017. At a slightly lower rate, groundwater As in Well B5 (41 m) has been rising steadily from $20 \mu\text{g/L}$ in October 2002 to $110 \mu\text{g/L}$ in December 2017 (Figure 6a; data since 2011 are shown). Rather than a thick clay layer, the transition between the shallow and intermediate aquifer at Site B is characterized by multiple thinner clay layers (Zheng et al., 2005). At the sandy Site T, As concentrations in one intermediate well (T3 at 52 m) screened near a peat layer have been fluctuating widely and rising since July 2015 (Figure 6b). Other monitoring wells in the intermediate aquifer in the study area show either constant

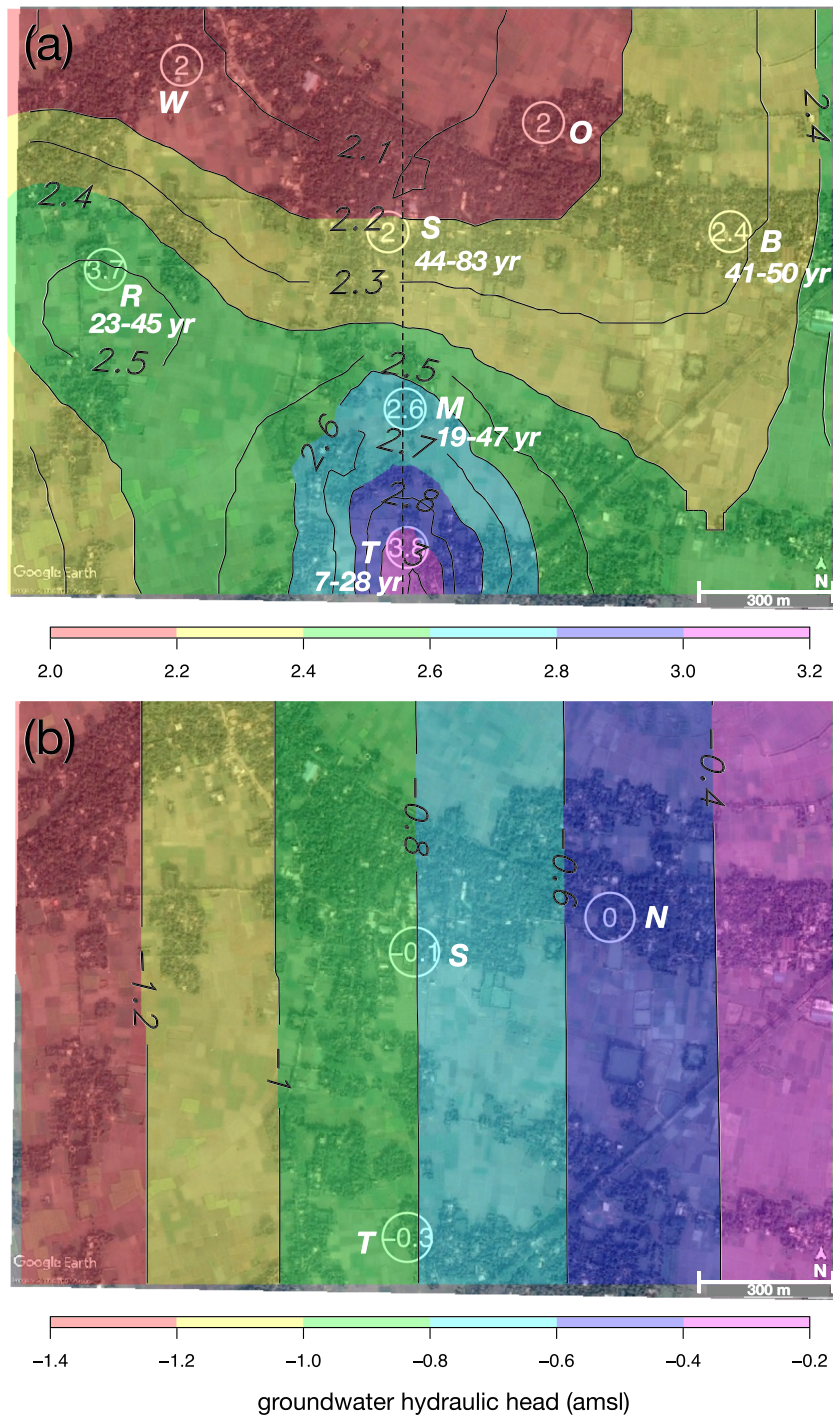


Figure 7. Simulated hydraulic heads in the study area. The simulated hydraulic heads above mean sea level (amsl) in the intermediate aquifer at 55-m depth (a) and deep aquifer at 195-m depth (b) under the current pumping condition. Simulated groundwater ages (yr) derived from reverse particle tracking results are also shown for the intermediate aquifer (a). Average observed heads (inside white circles) shown for a subset of intermediate wells (50–60 m deep) where long-term monitoring data are available and for three recently installed deep wells (195 m). The black dashed line in (a) is drawn along the south-north transect of Figure 8. A Google Earth image was used in the background.

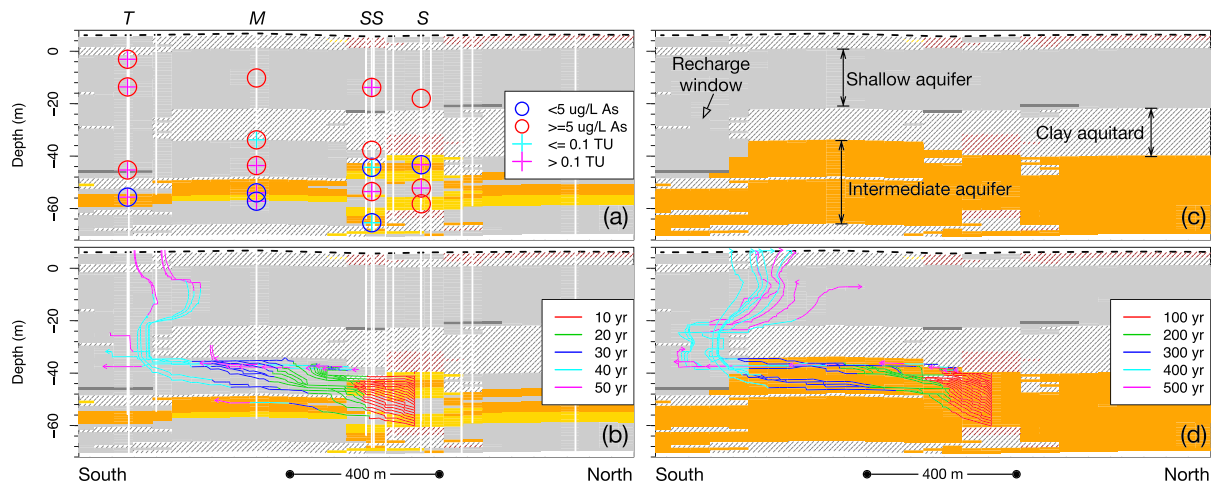


Figure 8. Tracing the source of groundwater and arsenic to the intermediate aquifer. A 2-D projection of the 3-D model along the S-N transect of Figure 7. The same cross-section is shown along a deeply scoured recharge window composed of Holocene, gray channel sand in juxtaposition with today's Pleistocene gray and orange sand (a and b) and a hypothetical Pleistocene aquifer composed of only orange sand under prepumping condition (c and d). The sections show (a) the distribution of As and tritium in shallow and intermediate aquifers along a lithological cross-section indicating the occurrence of gray and orange Pleistocene deposits; vertical white lines indicate drilling and/or groundwater monitoring locations; (b) flow paths of particles backward tracked for 50 yr from the As-contaminated, intermediate well nest that is located farthest from the recharge window; (c) previously uncontaminated, iron coated orange sand aquifer that is thought to be recently reduced due to the advection of shallow groundwater (a and b); the orange sand color throughout the Pleistocene aquifer is used for illustration purpose only; and (d) flow paths of particles backward tracked for 500 yr under no-pumping conditions. The dotted back line indicates surface elevation.

concentrations or variable concentrations of dissolved As without a clear trend or connection to seasonal variations in water level.

4.4. Groundwater Heads

The hydraulic head data are subdivided into shallow (8–40 m, $n = 17$), intermediate (40–90 m, $n = 30$), and deep (>90–195 m, $n = 5$) aquifer in accordance with the local stratigraphy. Seasonal variations in water level of about 4 m in amplitude parallel each other at different depths, with the highest heads recorded during the monsoon (August–September) and the lowest levels in March–April (Figure S13). In shallow and intermediate aquifer depths, water levels average 4.1 ± 0.2 ($\pm 1\sigma$) and 2.5 ± 0.8 m above mean sea level (amsl), respectively.

Across all locations, the average vertical head differences between a pair of shallow and intermediate wells from the same nest in clay-capped sites such as S, SS, and M (Figures 4f, 4l, 4r, and S13a) range between 1.3 and 2.8 m ($n = 21$) and average 2 ± 0.5 m. The corresponding vertical head gradient varies from 0.03 to 0.07. In contrast, the average vertical head differences between nested shallow and an intermediate depth wells at sandy sites such as T and R (Figures 5f, 5l, and S13b) range from 0.01 to 0.6 m ($n = 7$) and average 0.3 ± 0.2 m. The corresponding average vertical head gradient at the sandy sites is 0.01. There is a general trend of declining water levels in the intermediate aquifer as a function of increasing thickness of the confining clay aquitard in the study area (Figure S14).

The lateral distribution of hydraulic heads across the intermediate aquifer suggest groundwater flow from the sandy area in the south toward the clay-capped areas in the north. The average hydraulic head along the south-north transect within the intermediate aquifer (50–60 m bgs) decreases from about 3.8 m at the sandy site Well T3 to 2.6 m at the 12-m-thick clay-capped site Well M1–4a to 2 m at the 17-m clay-capped site Well S1 (Figures 4f, 4l, 4r, 5f, and 5l). Pressure transducer data indicate that the groundwater level in the deep aquifer is declining at a rate of 0.5 m/yr in the study area (Figure S13c).

4.5. Groundwater Flow Modeling

Groundwater flow modeling suggests that Dhaka pumping has significantly altered the groundwater flow system in this area, both regionally and locally. The model simulation of groundwater flow affected by

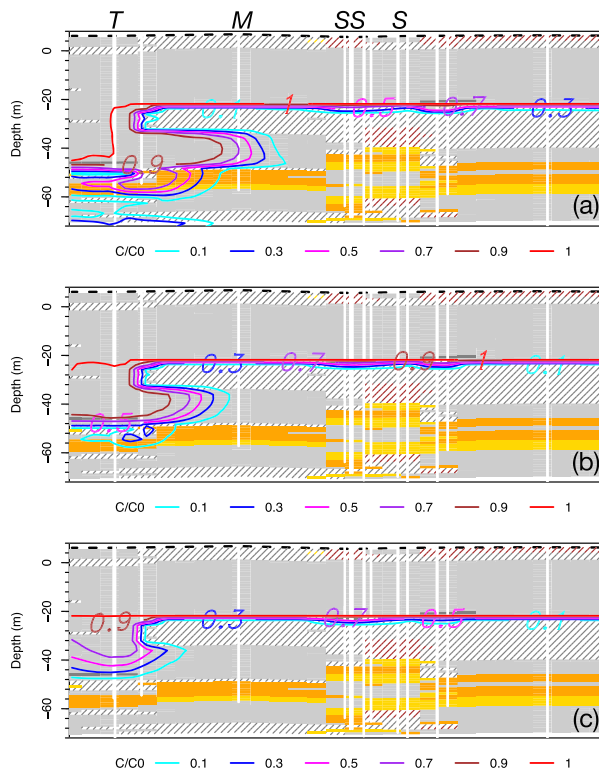


Figure 9. Arsenic transport with retardation under pumping. Simulated As distributions after 50 yr of pumping along a S-N transect (Figure 8a) for a retardation factor of (a) 3, (b) 10, and (c) 30.

pumping show a lateral hydraulic gradient driving south-north flow in the intermediate aquifer, and a strong vertical gradient between shallow and intermediate zones where the confining clay unit is present. Simulated heads in the portion of the intermediate aquifer without a clay cap are elevated compared to heads in the clay-capped portion of the aquifer along the central south to north transect in the area (Figure 7a). The highest simulated head was observed in the intermediate aquifer (55 m bgs) at the recharge window Site T. The simulated head drops by about 0.45 m at the clay-capped Site M (2.6 m amsl), 300 m north of Site T and by another 0.45 m at the clay-capped Site S (2.2 m amsl), 450 m north of Site M. The model predicts a high vertical gradient between the shallow and intermediate aquifer at the clay-capped sites (e.g., 0.08 at Site S). The local flow directions in the intermediate aquifer differ from the regional westerly flow within the deep aquifer (Figure 7).

Under prepumping conditions, the simulated groundwater heads in the intermediate aquifer are nearly invariant with local changes in geology. The prepumping simulation results along the T-M-S transect indicate a head drop of only 0.13 m over a distance of 750 m, corresponding to a lateral gradient of 0.00017 between Sites T and S, which is almost an order of magnitude lower than the simulated present day gradient of 0.0012. The simulated vertical head gradients across the confining unit under the prepumping scenario are 0.009 and 0.013 at the clay-capped Sites M and S, respectively, which is almost an order of magnitude lower than present day head gradients (0.05 and 0.08).

5. Discussion

Half of the 30 monitoring wells installed in the intermediate Pleistocene aquifer for this study were screened in gray sands and the other half in orange sands. With four exceptions, the intermediate wells installed in gray sand contained $>10 \mu\text{g/L}$ of As and wells installed in orange sand layers contain $\leq 5 \mu\text{g/L}$ of As (Table 1 and Figures 4 and 5). Sites S, SS, and eight other similar sites drilled in their vicinity indicate a high-As (measured at two sites), gray portion of the aquifer sandwiched between two layers of orange sand (Figures 4 and S4). Such inter-fingering of gray and orange sediment in the Pleistocene aquifer is an indication that layers that were once oxidized were probably reduced by lateral advection of reactive carbon with groundwater (Figure 8). We cannot rule out an alternation in preservation of orange, gray, followed again by orange sands over time, but lateral advection of high As and/or DOC water that reduced an originally orange sand layer provides a simpler explanation, as previously proposed in a different setting (van Geen et al., 2013).

The intrusion of shallow groundwater to the intermediate aquifer is confirmed by detectable (>0.1 TU) tritium (^3H) in 17 out of 30 monitoring wells screened between 41 and 72 m bgs (Table 2). Along today's predominant south-north flow path in the study area, ^3H was detected in 8 of the 11 analyzed intermediate monitoring wells at Sites T, M1, SS, and S (Figure 8a). The model predicts an average time frame of 15 ± 7 ($\pm 1\sigma$), 27 ± 7 , 32 ± 7 , and 60 ± 15 yr for shallow groundwater intrusion at Sites T, R, M, and S, respectively (Figure 7a), which is consistent with younger groundwater observed in sandy areas such as Site T (10–24 yr) and Site R (24–39 yr) and older groundwater in clay-capped areas such as Site M (11–69 yr) and Site S (45–47 yr) (Table 2). These results confirm the intrusion of shallow groundwater through discontinuities in the clay near sandy regions and lateral transport toward the clay-capped areas (Figure 8b). In comparison, the prepumping scenario predicts groundwater travel times that are about an order of magnitude longer along the same transect (Figures 8c and 8d).

A number of groundwater samples with $>10 \mu\text{g/L}$ As in the intermediate aquifer could not be dated because they did not contain ^3H . Of the five samples with $>10 \mu\text{g/L}$ As that could be dated using ^3H (S1, S2, R1, T3, and M4.5), S1 and M4.5 show a clear indication of mixing with older groundwater (Figure S12). This suggests that the release of As in portions of the intermediate aquifer is associated with fairly recent preferential flow.

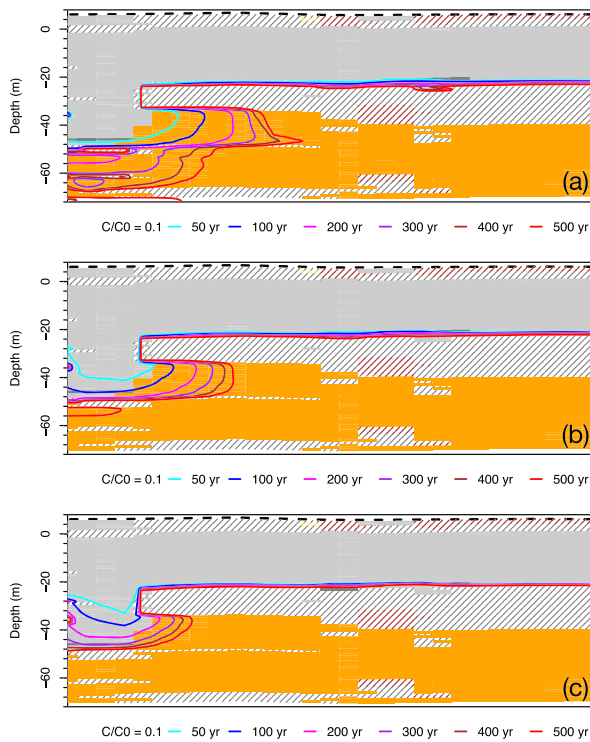


Figure 10. Arsenic transport with retardation under prepumping conditions. The simulated movement of the As front ($C/C_0 = 0.1$) along a S-N transect (Figure 8c) for a retardation factor of (a) 3, (b) 10, and (c) 30 after 50, 100, 200, 300, 400, and 500 yr of forward simulation.

The lack of a systematic relationship observed between ^3H , As, and sand color across sites (Figure 12) suggests that recent recharge of shallow groundwater in the intermediate aquifer is not the only mechanism that reduced Pleistocene orange sand to gray (Figures 8a and 8c) or increased groundwater As levels (Figure 6).

The model results suggest that recent advection of As from the shallow aquifer through the clay layer did not contaminate the Pleistocene aquifer that is distant from the recharge window (Figure 9). This is consistent with previous studies showing that As is significantly retarded relative to groundwater flow by adsorption to aquifer sands (BGS/DPHE, 2001; Dhar et al., 2011; Harvey et al., 2002; Itai et al., 2010; Jung et al., 2012; McArthur et al., 2011; Radloff et al., 2011, 2015; Robinson et al., 2011; Stollenwerk et al., 2007; Swartz et al., 2004; Thi Hoa Mai et al., 2014; van Geen et al., 2008, 2013). For a retardation factor of 10, for instance, the relative As concentration front (C/C_0) of 0.1 within the intermediate aquifer extends a maximum distance of 275 m north of the recharge area in 50 yr (Figure 9b). For a retardation factor of 30, which is more consistent with adsorption experiments conducted in the field (Radloff et al., 2011; van Geen et al., 2013), advection of high arsenic from the shallow aquifer to the measurement locations is even less likely (Figure 9c). Under the prepumping scenario, however, the simulated distribution of As today in the intermediate aquifer can be reproduced along the same transect if the model is run forward for about 400 yr (Figure 10).

With a retardation factor of 10, the proportion of the intermediate aquifer (>40–80 m bgs) that would be As contaminated ($C/C_0 \geq 0.1$) after 50 and 100 yr of pumping is estimated to be 7% and 16%, respectively (Figure 11). The simulations in three-dimensional space indicate that the plume of As would migrate downward through sandy recharge areas and would continue to propagate laterally in the semi-confined intermediate aquifer.

Intermediate wells near recharge windows are more vulnerable to the lateral intrusion of As from the shallow aquifer along the margins of the clay. Arsenic concentrations in wells that are further away from the recharge windows would therefore more likely be controlled by a local supply of reactive carbon. Thus, the proportion of the intermediate aquifer that is contaminated by pumping is expected to depend strongly on the spatial distribution of recharge windows.

There is evidence that advected DOC can be an important substrate for microbial reduction in aquifers and thus contributes to As mobilization. For example, previous studies have shown that the radiocarbon content

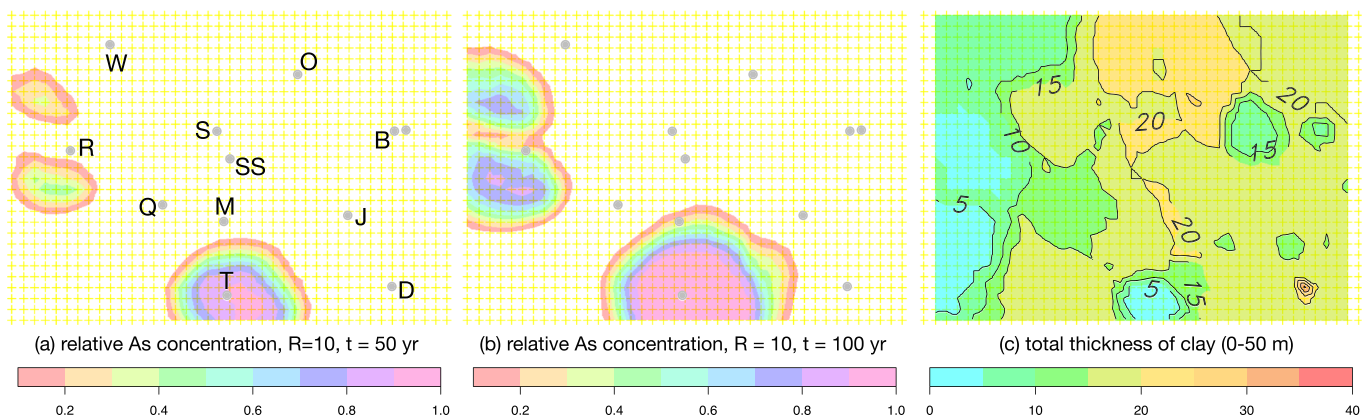


Figure 11. Intrusion of shallow groundwater arsenic (As) through breaks in the clay aquitard. Relative concentrations (C/C_0) of As at 52-m depth after (a) 50 yr and (b) 100 yr of forward simulation for a retardation factor (R) of 10 under the current pumping scenario; (c) the interpolated total thickness of clay from the surface to a depth of 50 m. Monitoring well locations screened between 50 and 60 m are shown in panel (a).

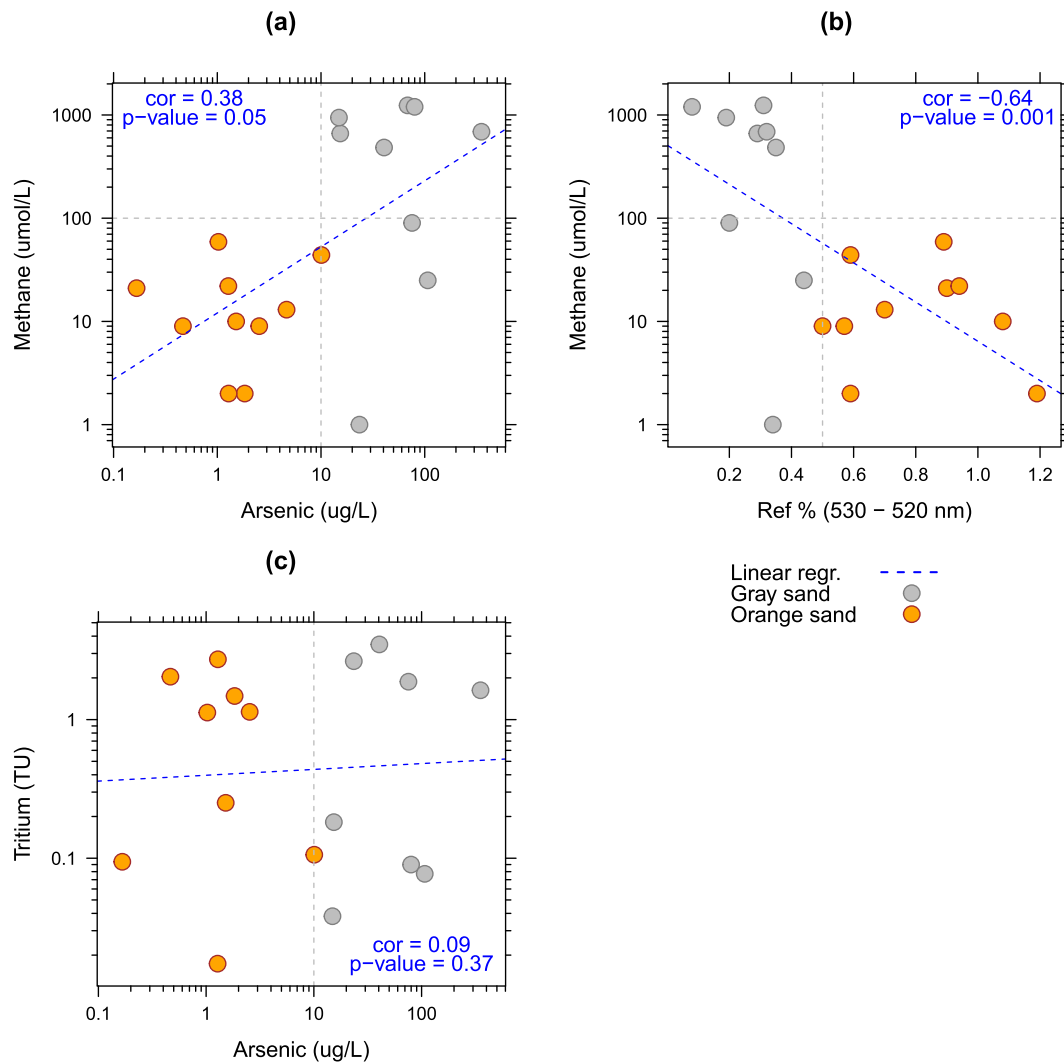


Figure 12. Correlation among dissolved methane (CH_4), arsenic (As), tritium (^3H), and diffuse spectral reflectance (530–520 nm) of screened depth sediment in the intermediate aquifer. Groundwater CH_4 concentrations are plotted as a function of As (a) and spectral reflectance (b). Groundwater ^3H concentrations (both detectable and non-detectable) are plotted as a function of As (c). The current detection limit for ^3H is 0.1 TU.

of labile bacterial DNA and phospholipid fatty acids in shallow aquifers of Araihaazar is closer to that of groundwater DOC than to that of organic carbon in the sediment (Mailloux et al., 2013; Whaley-Martin et al., 2016). Despite their high TOC content (12–50%), the peat or charcoal fragments encountered in 42% ($n = 33$) of the boreholes (Figure S4a), therefore, do not appear to be the main source of reactive carbon.

In our study area, the thick clay aquitard containing 1 order of magnitude higher DOC compared to the $<1\text{--}4$ mg/L DOC in the underlying intermediate aquifer (Figures 4b and 4n) could be an alternative source of carbon releasing As and reducing orange sand to gray (Mihajlov et al., 2020; Mozumder, 2019). The large vertical head gradients imposed by pumping in the clay-capped sites (Figures 4f, 4l, and 4r) could have accelerated the advective flux of DOC from the aquitard to the aquifer. Based on Darcy's flux in one-dimension, about 1.1 g of carbon/ m^2/yr is advected from the clay aquitard given an average pore-water DOC concentration of 20 mg/L (Figures 4b and 4n), a vertical hydraulic gradient of 0.2 across the clay aquitard (Figure 4f), a clay hydraulic conductivity value of 9×10^{-9} m/s, and an effective porosity of 0.3 for the sandy aquifer. Assuming that 1 mole of DOC is required to convert 4 moles of sedimentary Fe^{3+} to 4 moles of Fe^{2+} (Postma et al., 2007) and a reduction of 0.2% of the solid phase mass of Fe is enough to turn orange sand gray, the advective flux at a rate of 1.1 g of C/ m^2/yr is sufficient to convert 0.4 m of Fe^{3+} coated orange sand to gray sand over a time span of 50 yr.

Without the head gradient resulting from pumping (i.e., prepumping condition), the downward flux of DOC is controlled by molecular diffusion across the aquitard-aquifer interface (Mozumder, 2019). Calculations based on one-dimensional Fickian diffusion indicate that 0.016 g of C/m²/yr can be diffused from the clay aquitard to the intermediate aquifer assuming a diffusivity of 0.009 m²/yr (McMahon & Chapelle, 1991), a porosity of 0.5 for clay aquitard, and a DOC concentration gradient of 0.31 mM/m estimated across the aquifer-aquitard interface at Site M (Figures 4n and S15). Diffusion of DOC from clay can be extrapolated back in time by 5,000 yr assuming that anoxic conditions initiated 5,000–6,000 yr ago following the deposition of Holocene sand on the top of Holocene clay layers dated 8,800 ± 50 yr in the area (Figure S4b). At a rate of 0.016 g of C/m²/yr, 5,000 yr of integrated flux of diffused carbon is comparable to the advective influx of carbon induced by 50 yr of Dhaka pumping, resulting in the conversion of no more than 0.5 m of orange sand to gray. However, the average thickness of gray reduced sand directly underlying the thick clay in the area is 8 ± 6 m (Figure S4a), which is ~2 orders of magnitude greater than what could potentially be reduced by diffused or advected DOC from clay layers (Mihajlov et al., 2020). Thus, the extent of conversion from oxidized orange to reduced gray sand (Figures 8a and 8c) is likely due to a combination of DOC transport directly associated with clay layers and vertical/lateral transport of reactive carbon through sandy recharge windows in the study area.

Most field observations suggest that DOC is strongly adsorbed by sediments and retarded with respect to groundwater flow (Datta et al., 2011; Mailloux et al., 2013). Methane, on the other hand, does not adsorb (Cahill et al., 2017) and could be an alternative source of reactive carbon propagating at the same rate as groundwater flow (Figure S16). There is growing evidence that certain microorganisms oxidize CH₄ while reducing Fe oxides in the absence of sulfate (Amos et al., 2012; Ettwig et al., 2016). Concentrations of As and CH₄ generally track each other (correlation = 0.38 and *p*-value = 0.05) in the intermediate aquifer of our study area (Figure 12a). With three exceptions near sandy regions, about 50% of the wells tapping the gray Pleistocene sediment contain elevated levels of CH₄ (>200–1,239 μmol/L) whereas all wells tapping the orange Pleistocene aquifer contain very low levels of CH₄ (<60 μmol/L) (Table 3). In the clay-capped portion of the intermediate aquifer, in particular, high groundwater As is generally associated with elevated levels of CH₄ (Figures 4c, 4i, and 4o). The association of As relative to 10 μg/L, CH₄ relative to 100 μmol/L, and sand color relative to a 0.5% reflectance difference suggests that microbially mediated anaerobic oxidation of CH₄ by Fe oxides may have contributed to the release of As to the intermediate aquifer (Figure 12).

6. Conclusions

This detailed study based on direct field observations and modeling in a small area of Bangladesh sheds new light on the way local groundwater flow patterns affect groundwater As across a range of time scales. The combined observations suggest that the association of low As concentrations with oxidized Pleistocene sands was perturbed over thousands of years, before the onset of Dhaka pumping, mainly through local supply of reactive carbon. More recently, the expanding Dhaka drawdown cone magnified lateral and vertical head gradients determined by the heterogeneity in the local geology. Lateral transport of As, DOC, and/or CH₄ through breaks in a major clay aquitard could explain the elevated levels of As in reduced gray portions of the Pleistocene aquifer that are intercalated between layers that are still orange and oxidized. As a result of Dhaka pumping, an enhanced influx of reactive carbon accelerated the reduction of Fe oxides and the release of As to groundwater. In particular, the clay layer directly overlying the intermediate aquifer is a major source of reactive carbon, as evident from the recent rise in As near the aquifer-aquitard interface. Intermediate aquifers within the radius of influence of Dhaka pumping that have been tapped by a growing number of private households to reduce their exposure to As over the past decade are, therefore, vulnerable and need to be closely monitored.

References

- Ahmed, K. M., Bhattacharya, P., Hasan, M. A., Akhter, S. H., Alam, S. M. M., Bhuyian, M. A. H., et al. (2004). Arsenic enrichment in groundwater of the alluvial aquifers in Bangladesh: An overview. *Applied Geochemistry*, 19, 181–200.
- Ahmed, K. M., Hasan, M. K., Burgess, W. G., Dottridge, J., Ravenscroft, P., & van Wonderen, J. (1999). The Dupi Tila aquifer of Dhaka, Bangladesh: Hydraulic and hydrochemical response to intensive exploitation. In P. J. Chilton (Ed.), *Groundwater in the urban environment: Selected city profiles* (pp. 19–30). Available at: Rotterdam: Balkema. <http://discovery.ucl.ac.uk/169447/>

Acknowledgments

This study was financially supported primarily by HHS | NIH | National Institute of Environmental Health Sciences (NIEHS) Superfund Research Program Grant P42 ES010349 and National Science Foundation (NSF) Grant ICER1414131. We are grateful for the field support of many students and staffs affiliated with Dhaka University Geology Department. We are indebted to many villagers in Araihasar who generously offered their house yards for drilling and installation of monitoring wells. We are also thankful for the support of Bob Newton and Anthony Dachille during tritium and noble gas isotope analyses and Dennis Kent for his assistance with magnetic susceptibility analysis of the sediment cuttings. The geochemical data supporting the conclusions are provided in Tables 1, 2, and 3. The hydrologic data can be obtained online from CUAHSI Hydroshare (Mozumder, 2020). This is LDEO Contribution Number 8408.

- Ahmed K.M., Imam M. N., Akhter S. H., Hasan M. A., Alam M. M., Chowdhury S. Q., et al. (1998). Mechanism of arsenic release to groundwater: Geochemical and mineralogical evidence. In International Conference on Arsenic Pollution on Groundwater in Bangladesh: Causes, Effects, and Remedies. Dhaka Community Hospital, Dhaka, Bangladesh.
- Ahsan, H., Chen, Y., Parvez, F., Argos, M., Hussain, A. I., Momotaj, H., et al. (2006). Health Effects of Arsenic Longitudinal Study (HEALS): Description of a multidisciplinary epidemiologic investigation. *Journal of Exposure & Environmental Epidemiology*, *16*, 191–205.
- Amos, R. T., Bekins, B. A., Cozzarelli, I. M., Voytek, M. A., Kirshtein, J. D., Jones, E. J. P., & Blowes, D. W. (2012). Evidence for iron-mediated anaerobic methane oxidation in a crude oil-contaminated aquifer. *Geobiology*, *10*(6), 506–517. <https://doi.org/10.1111/j.1472-4669.2012.00341.x>
- Bayer, R., Schlosser, P., Bönisch, G., Rupp, H., Zaucker, F., & Zimmek, G. (1989). *Performance and blank components of a mass spectrometric system for routine measurement of helium isotopes and tritium by the ³He ingrowth method: Vorgelegt in der Sitzung vom 1. Juli 1989 von Otto Haxel*. Berlin Heidelberg: Springer-Verlag. www.springer.com/us/book/9783540517108
- BBS/UNICEF (2011). *Bangladesh National Drinking Water Quality Survey of 2009*. Dhaka: Bangladesh Bureau of Statistics and UNICEF.
- Berg, M., Tran, H. C., Nguyen, T. C., Pham, H. V., Schertenleib, R., & Giger, W. (2001). Arsenic contamination of groundwater and drinking water in Vietnam: A human health threat. *Environmental Science & Technology*, *35*(13), 2621–2626. <https://doi.org/10.1021/es010027y>
- BGS/DPHE (2001). *Arsenic contamination of groundwater in Bangladesh*. Keyword: BGS.
- Bhattacharya, P., Chatterjee, D., & Jacks, G. (1997). Occurrence of arsenic-contaminated groundwater in alluvial aquifers from delta plains, eastern India: Options for safe drinking water supply. *International Journal of Water Resources Development*, *13*, 79–92.
- Burgess, W. G., Hoque, M. A., Michael, H. A., Voss, C. I., Breit, G. N., & Ahmed, K. M. (2010). Vulnerability of deep groundwater in the Bengal Aquifer System to contamination by arsenic. *Nature Geoscience*, *3*, 83–87.
- Cahill, A. G., Steelman, C. M., Forde, O., Kuloyo, O., Ruff, S. E., Mayer, B., et al. (2017). Mobility and persistence of methane in groundwater in a controlled-release field experiment. *Nature Geoscience*, *10*, 289–294.
- Cheng, Z., Zheng, Y., Mortlock, R., & van Geen, A. (2004). Rapid multi-element analysis of groundwater by high-resolution inductively coupled plasma mass spectrometry. *Analytical and Bioanalytical Chemistry*, *379*, 512–518.
- Choudhury, I., Ahmed, K. M., Hasan, M., Mozumder, M. R. H., Knappett, P. S. K., Ellis, T., & van Geen, A. (2016). Evidence for elevated levels of arsenic in public wells of Bangladesh due to improper installation. *Groundwater*, *54*, 871–877.
- Datta, S., Neal, A. W., Mohajerin, T. J., Ocheltree, T., Rosenheim, B. E., White, C. D., & Johannesson, K. H. (2011). Perennial ponds are not an important source of water or dissolved organic matter to groundwaters with high arsenic concentrations in West Bengal, India. *Geophysical Research Letters*, *38*, L20404. <https://doi.org/10.1029/2011GL049301>
- Desbarats, A. J., Koenig, C. E. M., Pal, T., Mukherjee, P. K., & Beckie, R. D. (2014). Groundwater flow dynamics and arsenic source characterization in an aquifer system of West Bengal, India. *Water Resources Research*, *50*, 4974–5002. <https://doi.org/10.1002/2013WR014034>
- Desbarats, A. J., Pal, T., Mukherjee, P. K., & Beckie, R. D. (2017). Geochemical evolution of groundwater flowing through arsenic source sediments in an aquifer system of West Bengal, India. *Water Resources Research*, *53*, 8715–8735. <https://doi.org/10.1002/2017WR020863>
- Dhar, R. K., Zheng, Y., Saltikov, C. W., Radloff, K. A., Mailloux, B. J., Ahmed, K. M., & van Geen, A. (2011). Microbes enhance mobility of arsenic in Pleistocene aquifer sand from Bangladesh. *Environmental Science & Technology*, *45*(7), 2648–2654. <https://doi.org/10.1021/es1022015>
- Dhar, R. K., Zheng, Y., Stute, M., van Geen, A., Cheng, Z., Shanewaz, M., et al. (2008). Temporal variability of groundwater chemistry in shallow and deep aquifers of Araihasar, Bangladesh. *Journal of Contaminant Hydrology*, *99*(1–4), 97–111. <https://doi.org/10.1016/j.jconhyd.2008.03.007>
- Diamond, S. (1970). Pore size distributions in clays. *Clays and Clay Minerals*, *18*, 7–23.
- Elder, K. L., McNichol, A. P., & Gagnon, A. R. (1998). Reproducibility of seawater, inorganic and organic carbon ¹⁴C results at NOSAMS. *Radiocarbon*, *40*, 223–230.
- Ettwig, K. F., Zhu, B., Speth, D., Keltjens, J. T., Jetten, M. S. M., & Kartal, B. (2016). Archaea catalyze iron-dependent anaerobic oxidation of methane. *Proceedings of the National Academy of Sciences*, *113*, 12,792–12,796.
- Famiglietti, J. S. (2014). The global groundwater crisis. *Nature Climate Change*. Available at: <https://www.nature.com/articles/nclimate2425>
- Fendorf, S., Michael, H. A., & van Geen, A. (2010). Spatial and temporal variations of groundwater arsenic in South and Southeast Asia. *Science*, *328*(5982), 1123–1127. <https://doi.org/10.1126/science.1172974>
- Goodbred, S. L. Jr., & Kuehl, S. A. (2000). The significance of large sediment supply, active tectonism, and eustasy on margin sequence development: Late Quaternary stratigraphy and evolution of the Ganges–Brahmaputra delta. *Sedimentary Geology*, *133*, 227–248.
- Harbaugh A. W. (2005) MODFLOW-2005, the U.S. Geological Survey modular ground-water model—The ground-water flow process., U.S. Geological Survey.
- Harvey, C. F., Ashfaq, K. N., Yu, W., Badruzzaman, A. B. M., Ali, M. A., Oates, P. M., et al. (2006). Groundwater dynamics and arsenic contamination in Bangladesh. *Chemical Geology*, *228*, 112–136.
- Harvey, C. F., Swartz, C. H., Badruzzaman, A. B., Keon-Blute, N., Yu, W., Ali, M. A., et al. (2002). Arsenic mobility and groundwater extraction in Bangladesh. *Science*, *298*(5598), 1602–1606. <https://doi.org/10.1126/science.1076978>
- Hendry, M. J., Ranville, J. R., Boldt-Leppin, B. E. J., & Wassenaar, L. I. (2003). Geochemical and transport properties of dissolved organic carbon in a clay-rich aquitard. *Water Resources Research*, *39*(7), 1194. <https://doi.org/10.1029/2002WR001943>
- Hendry, M. J., & Schwartz, F. W. (1990). The chemical evolution of ground water in the Milk River aquifer, Canada. *Groundwater*, *28*, 253–261.
- Hendry, M. J., & Wassenaar, L. I. (2000). Controls on the distribution of major ions in pore waters of a thick surficial aquitard. *Water Resources Research*, *36*, 503–513.
- Hendry, M. J., & Wassenaar, L. I. (2005). Origin and migration of dissolved organic carbon fractions in a clay-rich aquitard: ¹⁴C and ^δ¹³C evidence. *Water Resources Research*, *41*, W02021. <https://doi.org/10.1029/2004WR003157>
- Hoque, M., Hoque, M. M., & Ahmed, K. (2007). Declining groundwater level and aquifer dewatering in Dhaka metropolitan area, Bangladesh: Causes and quantification. *Hydrogeology Journal*, *15*, 1523–1534.
- Hoque, M. A., & Burgess, W. G. (2012). ¹⁴C dating of deep groundwater in the Bengal Aquifer System, Bangladesh: Implications for aquifer anisotropy, recharge sources and sustainability. *Journal of Hydrology*, *444*, 209–220.
- Hoque, M. A., Burgess, W. G., & Ahmed, K. M. (2017). Integration of aquifer geology, groundwater flow and arsenic distribution in deltaic aquifers—A unifying concept. *Hydrological Processes*, *31*, 2095–2109.
- Hoque, M. A., Burgess, W. G., Shamsudduha, M., & Ahmed, K. M. (2011). Delineating low-arsenic groundwater environments in the Bengal Aquifer System, Bangladesh. *Applied Geochemistry*, *26*, 614–623.

- Horneman, A., Van Geen, A., Kent, D. V., Mathe, P. E., Zheng, Y., Dhar, R. K., et al. (2004). Decoupling of As and Fe release to Bangladesh groundwater under reducing conditions. Part 1: Evidence from sediment profiles. *Geochimica et Cosmochimica Acta*, *68*, 3459–3473.
- Hossain, M., Bhattacharya, P., Frappe, S. K., Jacks, G., Islam, M. M., Rahman, M. M., et al. (2014). Sediment color tool for targeting arsenic-safe aquifers for the installation of shallow drinking water tubewells. *Science of the Total Environment*, *493*, 615–625. <https://doi.org/10.1016/j.scitotenv.2014.05.064>
- Islam, F. S., Gault, A. G., Boothman, C., Polya, D. A., Charnock, J. M., Chatterjee, D., & Lloyd, J. R. (2004). Role of metal-reducing bacteria in arsenic release from Bengal delta sediments. *Nature*, *430*(6995), 68–71. <https://doi.org/10.1038/nature02638>
- Itai, T., Takahashi, Y., Seddique, A. A., Maruoka, T., & Mitamura, M. (2010). Variations in the redox state of As and Fe measured by X-ray absorption spectroscopy in aquifers of Bangladesh and their effect on As adsorption. *Applied Geochemistry*, *25*, 34–47.
- IWM and DWASA (2011). Establishment of groundwater monitoring system in Dhaka City for aquifer systems and DWASA production wells, Draft Final Report, Institute of Water Modeling and Dhaka Water Supply and Sewerage Authority, Dhaka.
- Jamil, N. B., Feng, H., Ahmed, K. M., Choudhury, I., Barnwal, P., & van Geen, A. (2019). Effectiveness of different approaches to arsenic mitigation over 18 years in Araihaazar, Bangladesh: Implications for national policy. *Environmental Science & Technology*, *53*, 5596–5604.
- Jung, H. B., Bostick, B. C., & Zheng, Y. (2012). Field, experimental, and modeling study of arsenic partitioning across a redox transition in a Bangladesh aquifer. *Environmental Science & Technology*, *46*(3), 1388–1395. <https://doi.org/10.1021/es2032967>
- Jusseret, S., Tam, V. T., & Dassargues, A. (2009). Groundwater flow modelling in the central zone of Hanoi, Vietnam. *Hydrogeology Journal*, *17*, 915–934.
- Khan, M. R., Koneshloo, M., Knappett, P. S. K., Ahmed, K. M., Bostick, B. C., Mailloux, B. J., et al. (2016). Megacity pumping and preferential flow threaten groundwater quality. *Nature Communications*, *7*, 12833.
- Khan, M. R., Michael, H. A., Nath, B., Huhmann, B. L., Harvey, C. F., Mukherjee, A., et al. (2019). High-arsenic groundwater in the southwestern Bengal Basin caused by a lithologically controlled deep flow system. *Geophysical Research Letters*, *46*, 13,062–13,071. <https://doi.org/10.1029/2019GL084767>
- Klump, S., Kipfer, R., Cirpka, O. A., Harvey, C. F., Brennwald, M. S., Ashfaque, K. N., et al. (2006). Groundwater dynamics and arsenic mobilization in Bangladesh assessed using noble gases and tritium. *Environmental Science & Technology*, *40*(1), 243–250. <https://doi.org/10.1021/es051284w>
- Knappett, P. S. K., Mailloux, B. J., Choudhury, I., Khan, M. R., Michael, H. A., Barua, S., et al. (2016). Vulnerability of low-arsenic aquifers to municipal pumping in Bangladesh. *Journal of Hydrology*, *539*, 674–686. <https://doi.org/10.1016/j.jhydrol.2016.05.035>
- Konikow, L. F., & Kendy, E. (2005). Groundwater depletion: A global problem. *Hydrogeology Journal*, *13*, 317–320.
- Lapworth, D. J., Zahid, A., Taylor, R. G., Burgess, W. G., Shamsudduha, M., Ahmed, K. M., et al. (2018). Security of deep groundwater in the coastal Bengal Basin revealed by tracers. *Geophysical Research Letters*, *45*, 8241–8252. <https://doi.org/10.1029/2018GL078640>
- Lawson, M., Polya, D. A., Boyce, A. J., Bryant, C., Mondal, D., Shantz, A., & Ballentine, C. J. (2013). Pond-derived organic carbon driving changes in arsenic hazard found in Asian groundwaters. *Environmental Science & Technology*, *47*(13), 7085–7094. <https://doi.org/10.1021/es400114q>
- Ludin, A., Weppernig, R., Bönisch, G., & Schlosser, P. (1998). Mass spectrometric measurement of helium isotopes and tritium in water samples. *41*.
- MacDonald, A. M., Bonsor, H. C., Ahmed, K. M., Burgess, W. G., Basharat, M., Calow, R. C., et al. (2016). Groundwater quality and depletion in the Indo-Gangetic Basin mapped from *in situ* observations. *Nature Geoscience*, *9*, 762–766.
- Mailloux, B. J., Trembath-Reichert, E., Cheung, J., Watson, M., Stute, M., Freyer, G. A., et al. (2013). Advection of surface-derived organic carbon fuels microbial reduction in Bangladesh groundwater. *Proceedings of the National Academy of Sciences*, *110*, 5331–5335.
- Manheim, F. T. (1966). A hydraulic squeezer for obtaining interstitial water from consolidated and unconsolidated sediments. *US Geological Survey Professional Paper*, *550.C*, 256–261.
- McArthur, J. M., Banerjee, D. M., Hudson-Edwards, K. A., Mishra, R., Purohit, R., Ravenscroft, P., et al. (2004). Natural organic matter in sedimentary basins and its relation to arsenic in anoxic ground water: The example of West Bengal and its worldwide implications. *Applied Geochemistry*, *19*, 1255–1293.
- McArthur, J. M., Ghosal, U., Sikdar, P. K., & Ball, J. D. (2016). Arsenic in groundwater: The deep Late Pleistocene aquifers of the Western Bengal Basin. *Environmental Science & Technology*, *50*(7), 3469–3476. <https://doi.org/10.1021/acs.est.5b02477>
- McArthur, J. M., Nath, B., Banerjee, D. M., Purohit, R., & Grassineau, N. (2011). Palaeosol control on groundwater flow and pollutant distribution: The example of arsenic. *Environmental Science & Technology*, *45*, 1376–1383.
- McArthur, J. M., Ravenscroft, P., Banerjee, D. M., Milsom, J., Hudson-Edwards, K. A., Sengupta, S., et al. (2008). How paleosols influence groundwater flow and arsenic pollution: A model from the Bengal Basin and its worldwide implication. *Water Resources Research*, *44*, W11411. <https://doi.org/10.1029/2007WR006552>
- McArthur, J. M., Ravenscroft, P., Safiulla, S., & Thirlwall, M. F. (2001). Arsenic in groundwater: Testing pollution mechanisms for sedimentary aquifers in Bangladesh. *Water Resources Research*, *37*, 109–117.
- McMahon, P. (2001). Aquifer/aquitard interfaces: Mixing zones that enhance biogeochemical reactions. *Hydrogeology Journal*, *9*, 34–43.
- McMahon, P. B., & Chapelle, F. H. (1991). Microbial production of organic acids in aquitard sediments and its role in aquifer geochemistry. *Nature*, *349*, 233–235.
- Michael, H. A., & Khan, M. R. (2016). Impacts of physical and chemical aquifer heterogeneity on basin-scale solute transport: Vulnerability of deep groundwater to arsenic contamination in Bangladesh. *Advances in Water Resources*, *98*, 147–158.
- Michael, H. A., & Voss, C. I. (2008). Evaluation of the sustainability of deep groundwater as an arsenic-safe resource in the Bengal Basin. *Proceedings of the National Academy of Sciences* Available at: <http://www.pnas.org/content/early/2008/06/16/0710477105>
- Michael, H. A., & Voss, C. I. (2009). Controls on groundwater flow in the Bengal Basin of India and Bangladesh: Regional modeling analysis. *Hydrogeology Journal*, *17*, 1561.
- Mihajlov I. (2014) The vulnerability of low-arsenic aquifers in Bangladesh: A multi-scale geochemical and hydrologic approach. Columbia University. Available at: <https://academiccommons.columbia.edu/doi/10.7916/D8K35RR6>
- Mihajlov, I., Mozumder, M. R. H., Bostick, B. C., Stute, M., Mailloux, B. J., Knappett, P. S. K., et al. (2020). Arsenic contamination of Bangladesh aquifers exacerbated by clay layers. *Nature Communications*. <https://doi.org/10.1038/s41467-020-16104-z>
- Mihajlov, I., Stute, M., Schlosser, P., Mailloux, B. J., Zheng, Y., Choudhury, I., et al. (2016). Recharge of low-arsenic aquifers tapped by community wells in Araihaazar, Bangladesh, inferred from environmental isotopes. *Water Resources Research*, *52*, 3324–3349. <https://doi.org/10.1002/2015WR018224>

- Mladenov, N., Zheng, Y., Miller, M. P., Nemerugut, D. R., Legg, T., Simone, B., et al. (2010). Dissolved organic matter sources and consequences for iron and arsenic mobilization in Bangladesh aquifers. *Environmental Science & Technology*, *44*(1), 123–128. <https://doi.org/10.1021/es901472g>
- Morgan, J. P., & McIntire, W. G. (1959). Quaternary geology of the Bengal basin, East Pakistan and India. *Geological Society of America Bulletin*, *70*, 319.
- Mozumder R. H. (2019). Impacts of pumping on the distribution of arsenic in Bangladesh groundwater. Columbia University. Available at: <https://doi.org/10.7916/d8-1w98-7737>
- Mozumder, R. H. (2020). Supporting hydrogeologic data of Araihaazar, Bangladesh. *HydroShare*, doi:10.4211/hs.c4c01c5f856546c3b2ddef15bf86c783
- Mukherjee, A., Fryar, A. E., Scanlon, B. R., Bhattacharya, P., & Bhattacharya, A. (2011). Elevated arsenic in deeper groundwater of the western Bengal basin, India: Extent and controls from regional to local scale. *Applied Geochemistry*, *26*, 600–613.
- Neumann, R. B., Ashfaq, K. N., Badruzzaman, A. B. M., Ashraf, A. M., Shoemaker, J. K., & Harvey, C. F. (2010). Anthropogenic influences on groundwater arsenic concentrations in Bangladesh. *Nature Geoscience*, *3*, 46–52.
- Nickson, R., McArthur, J., Burgess, W., Ahmed, K. M., Ravenscroft, P., & Rahman, M. (1998). Arsenic poisoning of Bangladesh groundwater. *Nature*, *395*, 338.
- Oremland, R. S., & Stolz, J. F. (2003). The ecology of arsenic. *Science*, *300*, 939–944.
- Oremland, R. S., & Stolz, J. F. (2005). Arsenic, microbes and contaminated aquifers. *Trends in Microbiology*, *13*(2), 45–49. <https://doi.org/10.1016/j.tim.2004.12.002>
- Pickering, J. L., Goodbred, S. L., Reitz, M. D., Hartzog, T. R., Mondal, D. R., & Hossain, M. S. (2014). Late Quaternary sedimentary record and Holocene channel avulsions of the Jamuna and Old Brahmaputra River valleys in the upper Bengal delta plain. *Geomorphology*, *227*, 123–136.
- Polizzotto, M. L., Harvey, C. F., Sutton, S. R., & Fendorf, S. (2005). Processes conducive to the release and transport of arsenic into aquifers of Bangladesh. *Proceedings of the National Academy of Sciences of the United States of America*, *102*, 18,819–18,823.
- Polizzotto, M. L., Kocar, B. D., Benner, S. G., Sampson, M., & Fendorf, S. (2008). Near-surface wetland sediments as a source of arsenic release to ground water in Asia. *Nature*, *454*(7203), 505–508. <https://doi.org/10.1038/nature07093>
- Pollock D. W. (2012). User guide for MODPATH version 6—A particle-tracking model for MODFLOW., USGS.
- Postma, D., Larsen, F., Minh Hue, N. T., Duc, M. T., Viet, P. H., Nhan, P. Q., & Jessen, S. (2007). Arsenic in groundwater of the Red River floodplain, Vietnam: Controlling geochemical processes and reactive transport modeling. *Geochimica et Cosmochimica Acta*, *71*, 5054–5071.
- Postma, D., Larsen, F., Thai, N. T., Trang, P. T. K., Jakobsen, R., Nhan, P. Q., et al. (2012). Groundwater arsenic concentrations in Vietnam controlled by sediment age. *Nature Geoscience*, *5*(9), 656–661.
- Postma, D., Mai, N. T. H., Lan, V. M., Trang, P. T. K., Sø, H. U., Nhan, P. Q., et al. (2017). Fate of arsenic during Red River water infiltration into aquifers beneath Hanoi, Vietnam. *Environmental Science & Technology*, *51*(2), 838–845. <https://doi.org/10.1021/acs.est.6b05065>
- Radloff, K. A., Zheng, Y., Michael, H. A., Stute, M., Bostick, B. C., Mihajlov, I., et al. (2011). Arsenic migration to deep groundwater in Bangladesh influenced by adsorption and water demand. *Nature Geoscience*, *4*(11), 793–798. <https://doi.org/10.1038/ngeo1283>
- Radloff, K. A., Zheng, Y., Stute, M., Weinman, B., Bostick, B., Mihajlov, I., et al. (2015). Reversible adsorption and flushing of arsenic in a shallow, Holocene aquifer of Bangladesh. *Applied Geochemistry* Available at: <http://www.sciencedirect.com/science/article/pii/S0883292715300706>
- Ravenscroft, P., Brammer, H., & Richards, K. (2009). *Arsenic pollution: A global synthesis*. UK: John Wiley & Sons, Ltd. Available at: <https://doi.org/10.1002/9781444308785>
- Ravenscroft, P., Kabir, A., Hakim, S. A. I., Ibrahim, A. K. M., Ghosh, S. K., Rahman, M. S., et al. (2014). Effectiveness of public rural waterpoints in Bangladesh with special reference to arsenic mitigation. *Journal of Water, Sanitation and Hygiene for Development*, *4*, 545–562.
- Ravenscroft, P., McArthur, J. M., & Hoque, M. A. (2013). Stable groundwater quality in deep aquifers of southern Bangladesh: The case against sustainable abstraction. *Science of Total Environment*, *454–455*, 627–638.
- Ravenscroft, P., McArthur, J. M., & Rahman, M. S. (2018). Identifying multiple deep aquifers in the Bengal Basin: Implications for resource management. *Hydrological Processes*, *32*, 3615–3632.
- Robinson, C., Brömssen, M., von Bhattacharya, P., Häller, S., Bivén, A., Hossain, M., et al. (2011). Dynamics of arsenic adsorption in the targeted arsenic-safe aquifers in Matlab, south-eastern Bangladesh: Insight from experimental studies. *Applied Geochemistry*, *26*, 624–635.
- Rotiroli, M., Sacchi, E., Fumagalli, L., & Bonomi, T. (2014). Origin of arsenic in groundwater from the multilayer aquifer in Cremona (northern Italy). *Environmental Science & Technology*, *48*(10), 5395–5403. <https://doi.org/10.1021/es405805v>
- Rowland, H. A. L., Pederick, R. L., Polya, D. A., Pancost, R. D., Van Dongen, B. E., Gault, A. G., et al. (2007). The control of organic matter on microbially mediated iron reduction and arsenic release in shallow alluvial aquifers, Cambodia. *Geobiology*, *5*, 281–292.
- Sahu, P., Michael, H. A., Voss, C. I., & Sikdar, P. K. (2013). Impacts on groundwater recharge areas of megacity pumping: Analysis of potential contamination of Kolkata, India, water supply. *Hydrological Sciences Journal*, *58*, 1340–1360.
- Shamsudduha, M., Taylor, R. G., Ahmed, K. M., & Zahid, A. (2011). The impact of intensive groundwater abstraction on recharge to a shallow regional aquifer system: Evidence from Bangladesh. *Hydrogeology Journal*, *19*, 901–916.
- Shamsudduha, M., Taylor, R. G., & Chandler, R. E. (2015). A generalized regression model of arsenic variations in the shallow groundwater of Bangladesh. *Water Resources Research*, *51*, 685–703. <https://doi.org/10.1002/2013WR014572>
- Shamsudduha, M., Zahid, A., & Burgess, W. G. (2019). Security of deep groundwater against arsenic contamination in the Bengal Aquifer System: A numerical modeling study in southeast Bangladesh. *Sustainable Water Resources Management*, *5*, 1073–1087.
- Simpkins, W. W., & Parkin, T. B. (1993). Hydrogeology and redox geochemistry of CH₄ in a Late Wisconsinan Till and Loess Sequence in central Iowa. *Water Resources Research*, *29*, 3643–3657.
- Smith, A. H., Elena, O., & Lingas and Rahman M. (2000). Contamination of drinking-water by arsenic in Bangladesh: A public health emergency. *Bulletin of the World Health Organization*, *78*(9), 1093–1103.
- Stahl, M. O., Harvey, C. F., Geen, A., van Sun, J., Trang, P. T. K., Lan, V. M., et al. (2016). River bank geomorphology controls groundwater arsenic concentrations in aquifers adjacent to the Red River, Hanoi Vietnam. *Water Resources Research*, *52*, 6321–6334. <https://doi.org/10.1002/2016WR018891>
- Stollenwerk, K. G., Breit, G. N., Welch, A. H., Yount, J. C., Whitney, J. W., Foster, A. L., et al. (2007). Arsenic attenuation by oxidized aquifer sediments in Bangladesh. *Science of the Total Environment*, *379*(2-3), 133–150. <https://doi.org/10.1016/j.scitotenv.2006.11.029>

- Stute, M., Zheng, Y., Schlosser, P., Horneman, A., Dhar, R. K., Datta, S., et al. (2007). Hydrological control of As concentrations in Bangladesh groundwater. *Water Resources Research*, 43, W09417. <https://doi.org/10.1029/2005WR004499>
- Swartz, C. H., Blute, N. K., Badruzzaman, B., Ali, A., Brabander, D., Jay, J., et al. (2004). Mobility of arsenic in a Bangladesh aquifer: Inferences from geochemical profiles, leaching data, and mineralogical characterization. *Geochimica et Cosmochimica Acta*, 68, 4539–4557.
- Thi Hoa Mai, N., Postma, D., Thi Kim Trang, P., Jessen, S., Hung, V. P., & Larsen, F. (2014). Adsorption and desorption of arsenic to aquifer sediment on the Red River floodplain at Nam Du, Vietnam. *Geochimica et Cosmochimica Acta*, 142, 587–600.
- Umitsu, M. (1994). Late quaternary sedimentary environments and landforms in the Ganges Delta. *Sedimentary Geology*, 83, 177–186.
- van Geen, A., Ahmed, E. B., Pitcher, L., Mey, J. L., Ahsan, H., Graziano, J. H., & Ahmed, K. M. (2014). Comparison of two blanket surveys of arsenic in tubewells conducted 12 years apart in a 25 km² area of Bangladesh. *Science of the Total Environment*, 488–489, 484–492.
- van Geen, A., Bostick, B. C., Thi Kim Trang, P., Lan, V. M., Mai, N.-N., Manh, P. D., et al. (2013). Retardation of arsenic transport through a Pleistocene aquifer. *Nature*, 501(7466), 204–207. <https://doi.org/10.1038/nature12444>
- van Geen, A., Cheng, Z., Jia, Q., Seddique, A. A., Rahman, M. W., Rahman, M. M., & Ahmed, K. M. (2007). Monitoring 51 community wells in Araihaazar, Bangladesh, for up to 5 years: Implications for arsenic mitigation. *Journal of Environment Science Health Part A*, 42, 1729–1740.
- van Geen, A., Rose, J., Thoral, S., Garnier, J. M., Zheng, Y., & Bottero, J. Y. (2004). Decoupling of As and Fe release to Bangladesh groundwater under reducing conditions. Part II: Evidence from sediment incubations. *Geochimica et Cosmochimica Acta*, 68, 3475–3486.
- van Geen, A., Trevisani, M., Immel, J., Jakariya, M., Osman, N., Cheng, Z., et al. (2006). Targeting low-arsenic groundwater with mobile-phone technology in Araihaazar, Bangladesh. *Journal of Health, Population, and Nutrition*, 24, 282–297.
- van Geen, A., Zheng, Y., Goodbred, S., Horneman, A., Aziz, Z., Cheng, Z., et al. (2008). Flushing history as a hydrogeological control on the regional distribution of arsenic in shallow groundwater of the Bengal Basin. *Environmental Science & Technology*, 42(7), 2283–2288. <https://doi.org/10.1021/es702316k>
- van Geen, A., Zheng, Y., Versteeg, R., Stute, M., Horneman, A., Dhar, R., et al. (2003). Spatial variability of arsenic in 6000 tube wells in a 25 km² area of Bangladesh. *Water Resources Research*, 39(5), 1140. <https://doi.org/10.1029/2002WR001617>
- von Brömssen, M., Jakariya, M., Bhattacharya, P., Ahmed, K. M., Hasan, M. A., Sracek, O., et al. (2007). Targeting low-arsenic aquifers in Matlab Upazila, Southeastern Bangladesh. *Science of the Total Environment*, 379, 121–132.
- von Brömssen, M., Markussen, L., Bhattacharya, P., Ahmed, K. M., Hossain, M., Jacks, G., et al. (2014). Hydrogeological investigation for assessment of the sustainability of low-arsenic aquifers as a safe drinking water source in regions with high-arsenic groundwater in Matlab, southeastern Bangladesh. *Journal of Hydrology*, 518, 373–392.
- Wada, Y., Beek, L. P. H., van Kempen, C. M., van Reckman, J. W. T. M., Vasak, S., & Bierkens, M. F. P. (2010). Global depletion of groundwater resources. *Geophysical Research Letters*, 37, L20402. <https://doi.org/10.1029/2010GL044571>
- Walker, S. A., Azetsu-Scott, K., Normandeau, C., Kelley, D. E., Friedrich, R., Newton, R., et al. (2016). Oxygen isotope measurements of seawater (18O/16O): A comparison of cavity ring-down spectroscopy (CRDS) and isotope ratio mass spectrometry (IRMS). *Limnology and Oceanography: Methods*, 14, 31–38.
- Weinman, B., Goodbred, S. L., Zheng, Y., Aziz, Z., Steckler, M., van Geen, A., et al. (2008). Contributions of floodplain stratigraphy and evolution to the spatial patterns of groundwater arsenic in Araihaazar, Bangladesh. *Geological Society of America Bulletin*, 120, 1567–1580.
- Werner, A. D., Zhang, Q., Xue, L., Smerdon, B. D., Li, X., Zhu, X., et al. (2013). An initial inventory and indexation of groundwater mega-depletion cases. *Water Resources Management*, 27, 507–533.
- Whaley-Martin K. J. (2017). Examining microbial carbon source cycling in arsenic contaminated Bangladesh aquifers through lipid and isotopic analyses. McMaster University.
- Whaley-Martin, K. J., Mailloux, B. J., van Geen, A., Bostick, B. C., Silvern, R. F., Kim, C., et al. (2016). Stimulation of microbially mediated arsenic release in Bangladesh aquifers by young carbon indicated by radiocarbon analysis of sedimentary bacterial lipids. *Environmental Science & Technology*, 50(14), 7353–7363. <https://doi.org/10.1021/acs.est.6b00868>
- WHO (1993). *Guidelines for drinking-water quality*. Geneva. Available at: World Health Organization. <http://apps.who.int/iris/bitstream/handle/10665/259956/9241544600-eng.pdf;jsessionid=6A88AB5DA4633E395E762B07AC27953A?sequence=1>
- Winkel, L. H. E., Trang, P. T. K., Lan, V. M., Stengel, C., Amini, M., Ha, N. T., et al. (2011). Arsenic pollution of groundwater in Vietnam exacerbated by deep aquifer exploitation for more than a century. *Proceedings of the National Academy of Sciences*, 108, 1246–1251.
- Winston, R.B., (2019). ModelMuse version 4—A graphical user interface for MODFLOW 6: U.S. Geological Survey Scientific Investigations Report 2019–5036, 10 p.
- Zheng, C., & Wang, P. P. (1999). *MT3DMS: A modular three-dimensional multispecies transport model for simulation of advection, dispersion, and chemical reactions of contaminants in groundwater systems; documentation and user's guide*. Tuscaloosa, Alabama, USA. Available at: University of Alabama prepared for US Army Corps of Engineers. <http://www.dtic.mil/dtic/tr/fulltext/u2/a373474.pdf>
- Zheng, Y., van Geen, A., Stute, M., Dhar, R., Mo, Z., Cheng, Z., et al. (2005). Geochemical and hydrogeological contrasts between shallow and deeper aquifers in two villages of Araihaazar, Bangladesh: Implications for deeper aquifers as drinking water sources. *Geochimica et Cosmochimica Acta*, 69, 5203–5218.

References From the Supporting Information

- Burnol, A., Garrido, F., Baranger, P., Joulain, C., Dictor, M.-C., Bod Bod, F., et al. (2007). Decoupling of arsenic and iron release from ferrihydrite suspension under reducing conditions: A biogeochemical model. *Geochemical Transactions*, 8, 12.
- Gonthier, G.J., (2007). A graphical method for estimation of barometric efficiency from continuous data—Concepts and applications to a site in the Piedmont, Air Force Plant 6, Marietta, Georgia. *U.S. Geological Survey Scientific Investigations Report 2007-5111*, Reston, Virginia.